Fall 2010

Quantification of uncertainty in aerodynamic heating of a reentry vehicle due to uncertain wall and freestream conditions

Benjamin R. Bettis

Department:

QUANTIFICATION OF UNCERTAINTY IN AERODYNAMIC HEATING OF A REENTRY VEHICLE DUE TO UNCERTAIN WALL AND FREESTREAM CONDITIONS

by

BENJAMIN ROBERT BETTIS

A THESIS

Presented to the Faculty of the Graduate School of the

MISSOURI UNIVERSITY OF SCIENCE AND TECHNOLOGY

in Partial Fulfillment of the Requirements for the Degree

MASTER OF SCIENCE IN AEROSPACE ENGINEERING

2010

Approved by

Dr. Serhat Hosder, Advisor
Dr. David W. Riggins
Dr. Xiaoping Du

ABSTRACT

The primary focus of this study is to demonstrate an efficient approach for uncertainty quantification of surface heat flux to the spherical non-ablating heat-shield of a generic reentry vehicle due to epistemic and aleatory uncertainties that may exist in various parameters used in the numerical solution of hypersonic, viscous, laminar blunt-body flows with thermo-chemical non-equilibrium. Two main uncertainty sources were treated in the computational fluid dynamics (CFD) simulations: (1) aleatory uncertainty in the freestream velocity and (2) epistemic uncertainty in the recombination efficiency for a partially catalytic wall boundary condition. The Second-Order Probability utilizing a stochastic response surface obtained with Point-Collocation Non-Intrusive Polynomial Chaos was used for the propagation of mixed (aleatory and epistemic) uncertainties. The uncertainty quantification approach was validated on a stochastic model problem with mixed uncertainties for the prediction of stagnation point heat transfer with Fay-Riddell relation, which included the comparison with direct Monte Carlo sampling results. In the stochastic CFD problem, the uncertainty in surface heat transfer was obtained in terms of intervals at different probability levels at various locations including the stagnation point and the shoulder region. The mixed uncertainty results were compared to the results obtained with a purely aleatory uncertainty analysis to show the difference between two uncertainty quantification approaches. A global sensitivity analysis indicated that the velocity has a stronger contribution to the overall uncertainty in the stagnation point heat transfer for the range of input uncertainties considered in this study.

ACKNOWLEDGMENT

I would like to express my heartfelt appreciation for my advisor Dr. Serhat Hosder and thank him for the opportunity to conduct this research project under his supervision and guidance. He has been a great inspiration to me, and has helped me tremendously over the past few years. Thank you very much for the time you have invested in teaching and grooming me to become a better researcher.

I would also like to thank my committee members; Dr. David Riggins and Dr. Xiaoping Du for their knowledge they have bestowed upon me through the courses they teach and also for their insights and time spent on reviewing my thesis. Furthermore, I would like to thank Dr. Serhat Hosder and Dr. David Riggins for their time and efforts in composing reference letters for me which has undoubtedly given me more funding opportunities.

I also want to thank the Missouri University of Science and Technology and the Aerospace Engineering Department for the educational process and development they have provided me with over the past five years. Furthermore, I want to thank Yi Zhang, Srikanth Adya, and Daoru Han for all of their support while working together in the Computational Fluid Dynamics and Aerospace Design Laboratory.

I would like to thank the Missouri University of Science and Technology Chancellor's Fellowship, NASA Missouri Space Grant Consortium, NASA STTR Grant NNX10CF64P, and the NASA Aeronautics Scholarship Program for their support and funding throughout my graduate career.

Finally, I want to thank my family for their love and support. I feel truly blessed to have such a loving family.

TABLE OF CONTENTS

Page

ABSTRACT iii

ACKNOWLEDGMENT iv

LIST OF ILLUSTRATIONS vii

LIST OF TABLES ix

NOMENCLATURE x

SECTION

1. INTRODUCTION 1

1.1. MOTIVATION FOR UNCERTAINTY QUANTIFICATION 1

1.2. OBJECTIVES OF THE CURRENT STUDY 2

1.3. CONTRIBUTIONS OF THE CURRENT STUDY 3

1.4. THESIS OUTLINE 4

2. LITERATURE REVIEW 6

2.1. MIXED UNCERTAINTY QUANTIFICATION 6

2.2. HYPERSONIC VEHICLE APPLICATIONS 9

3. UNCERTAINTY QUANTIFICATION APPROACH 11

3.1. UNCERTAINTIES IN COMPUTATIONAL SIMULATIONS 11

3.2. MIXED UNCERTAINTY PROPAGATION 13

3.2.1. Second-Order Probability 14

3.2.2. Basics of Polynomial Chaos 14

3.2.3. Point-Collocation Non-Intrusive Polynomial Chaos 19

3.2.4. Implementation of NIPC in Second-Order Probability 20

4. STOCHASTIC MODEL PROBLEM 22

4.1. DESCRIPTION OF FAY-RIDDELL CORRELATION 22

4.1.1. Calculation of Properties Across a Normal Shock Wave 22

4.1.2. Mass Fraction Calculation for Air 25

4.1.3. Fay-Riddell Correlation 29
4.2. DESCRIPTION OF THE STOCHASTIC PROBLEM 32
4.3. MIXED UNCERTAINTY QUANTIFICATION 34
4.4. SENSITIVITY ANALYSIS 38
5. UNCERTAINTY QUANTIFICATION IN CFD SIMULATIONS 42
5.1. INTRODUCTION TO COMPUTATIONAL FLUID DYNAMICS 42
5.2. COMPUTATIONAL MODELING 43
5.2.1. CFD Solver and Numerical Scheme 43
5.2.2. Boundary Conditions 44
5.2.3. Physics Modeling 45
5.2.4. Computational Grid 46
5.3. DESCRIPTION OF THE STOCHASTIC PROBLEM 47
5.4. UNCERTAINTY QUANTIFICATION IN AEROHEATING 49
5.4.1. Results with Purely Aleatoric Uncertainty Assumption 49
5.4.2. Results with Mixed (Aleatory-Epistemic) Uncertainty Assumption 52
5.5. SENSITIVITY ANALYSIS 57
6. CONCLUSIONS AND FUTURE WORK 60
6.1. CONCLUSIONS 60
6.2. FUTURE WORK 61
APPENDICES
A. Thermodynamic Curve-fits: MATLAB Source Code 64
B. Statistical Thermodynamics 73
C. Fay-Riddell Model Problem: MATLAB Source Code 79
D. Uncertainty Quantification MATLAB Source Code 86
BIBLIOGRAPHY 91
VITA 95

LIST OF ILLUSTRATIONS

Figure Page

3.1 Sample probability density functions of common statistical distributions. . 12

3.2 Schematic of second-order probability. 15

3.3 Flowchart describing the procedure for propagating mixed aleatory-epistemic uncertainties with Second-Order Probability and NIPC response surface. . 21

4.1 Variation of coefficient of viscosity as a function of temperature and pressure (Anderson [29]). 33

4.2 Convergence of the average stagnation point heat transfer. 35

4.3 Convergence of the standard deviation of stagnation point heat transfer. . 36

4.4 Horse-tail plot representing mixed aleatory-epistemic uncertainty results for the Fay-Riddell model problem (uniform distribution for velocity). . . . 36

4.5 Horse-tail plot representing mixed aleatory-epistemic uncertainty results for the Fay-Riddell model problem (normal distribution for velocity). 37

4.6 Correlation plots demonstrating the influence of velocity on the overall uncertainty in the stagnation heat flux with velocity following a uniform distribution. 40

4.7 Correlation plots demonstrating the influence of k ($k = \mu_e/\mu_{e_{ref}}$) on the overall uncertainty in the stagnation heat flux with velocity following a uniform distribution. 40

4.8 Correlation plots demonstrating the influence of velocity on the overall uncertainty in the stagnation heat flux with velocity following a normal distribution. 41

4.9 Correlation plots demonstrating the influence of k ($k = \mu_e/\mu_{e_{ref}}$) on the overall uncertainty in the stagnation heat flux with velocity following a normal distribution. 41

5.1 CFD solution for surface heating for fully-catalytic and non-catalytic wall boundary condition. 45

5.2 Geometry and coordinate nomenclature for the reentry vehicle used in the experiments by MacLean et al. [2] 47

5.3 Computational grid for the 2-D axis-symmetric spherical capsule. 47

5.4 Pressure contour plot indicating a converged CFD solution. 48

5.5 Convergence of NIPC response surface. 50

5.6 PDF curve for 5^{th} order NIPC. 51

5.7 NIPC response surface (p = 5). 52

5.8 Mean and 95% C.I. for surface heat flux distribution (purely aleatoric uncertainty assumption). 52

5.9 Second-Order Probability results for surface heat transfer at the stagnation point..... 53

5.10 Second-Order Probability results for surface heat transfer at the shoulder region. 53

5.11 Comparison of pure aleatory and mixed aleatory-epistemic uncertainty results for surface heat transfer (Probability level 2.5%). 56

5.12 Comparison of pure aleatory and mixed aleatory-epistemic uncertainty results for surface heat transfer (Probability level 50%). 56

5.13 Comparison of pure aleatory and mixed aleatory-epistemic uncertainty results for surface heat transfer (Probability level 97.5%). 57

5.14 Correlation plots demonstrating the influence of velocity on the overall uncertainty in the stagnation heat flux. 59

5.15 Correlation plots demonstrating the influence of $log_{10}(\gamma)$ on the overall uncertainty in the stagnation heat flux. 59

LIST OF TABLES

Table Page

3.1 Density and weight functions associated with several commonly used univariate optimal bases functions. 16

4.1 Table outlining the free stream conditions for the CFD (Case 1) and the model problem (Case 2). 32

4.2 Stagnation point heat transfer (W/cm^2) at different probability levels for the model problem (Free-stream velocity is taken as a uniform random variable). 37

4.3 Stagnation point heat transfer (W/cm^2) at different probability levels for the model problem (Free-stream velocity is taken as a normal random variable). 38

5.1 Surface heat transfer (W/cm^2) for the stagnation point and the shoulder region at different probability levels for the CFD problem. 54

NOMENCLATURE

Symbol	Description
c	Mass fraction
e	Boundary layer edge (subscript)
h	Enthalpy ($J/kg{\cdot}^{\circ}K$)
Le	Lewis number
n	Number of random variables
o	Total or stagnation condition (subscript)
p	Pressure (N/m^2)
Pr	Prandtl number
R_N	Radius of curvature (m)
sp	Stagnation point (subscript)
T	Temperature (K)
V	Velocity (m/s)
w	Wall (subscript)
α	Spectral modes
α^*	Stochastic output variable
γ	Recombination efficiency
Δh_f	Heat of formation ($J/kg{\cdot}K$)
μ	Coefficient of viscosity ($kg/m{\cdot}s$)
ξ	Standard random variable
$\vec{\xi}_a$	Standard aleatory uncertain variable
$\vec{\xi}_e$	Standard epistemic uncertain variable
ρ	Density (kg/m^3)
Ψ	Random basis function
∞	Freestream (subscript)

1. INTRODUCTION

1.1. MOTIVATION FOR UNCERTAINTY QUANTIFICATION

Uncertainties are generally ubiquitous in the analysis and design of highly complex engineering systems. Uncertainties can arise from the lack of knowledge in physical modeling (epistemic uncertainty), inherent variations in the systems (aleatory uncertainty), and numerical errors in the computational procedures used for analysis. It is important to account for these uncertainties in applications such as robust and reliable design of multi-disciplinary aerospace systems. One application is the design of a thermal protection system (TPS) for an atmospheric reentry vehicle. Orbital vehicles travel at very high velocities when reentering the Earth's atmosphere and will experience a significant magnitude of aeroheating. In order to design and fabricate a reliable TPS for a reentry vehicle, engineers must have a tool set for accurate prediction of the surface heat flux during atmospheric reentry. Due to the high enthalpy and velocity requirements for most hypersonic flow simulations including reentry flows, there are few facilities where experiments can be performed. These experiments also cover a limited reentry envelope with very small operating times. Therefore, computational fluid dynamics (CFD) methods play an important role in the prediction of the flow field and the surface heat flux for atmospheric reentry, and for hypersonic applications in general. Accurate numerical prediction of hypersonic flow fields are challenging due to the complex nature of the physics such as strong shock waves, viscous shock layers, and non-equilibrium thermo-chemistry. Various uncertainties associated with high-fidelity hypersonic flow simulations can have significant effects

on the accuracy of the results including the surface heat flux. Therefore, it is important to include these uncertainties in the simulations to assess the accuracy of the results and to obtain robust and/or reliable reentry vehicle designs.

1.2. OBJECTIVES OF THE CURRENT STUDY

The primary focus of this study was to demonstrate an efficient approach for uncertainty quantification of surface heat flux to the spherical non-ablating heat-shield of a reentry vehicle at zero-angle of attack due to epistemic and aleatory uncertainties that may exist in various parameters used in the numerical solution of hypersonic, viscous, laminar blunt-body flows with thermo-chemical non-equilibrium. In specific, the freestream velocity (V_∞) and the recombination efficiency (γ) of oxygen and nitrogen atoms used in the description of catalytic wall boundary condition [1] were treated as uncertain variables. A recent work by MacLean et al. [2], which included both experimental and numerical studies on the hypersonic aerodynamic heating of spherical capsule geometries, demonstrated a significant variation of the surface heat-flux with varying recombination efficiencies (e.g., catalytic wall conditions) and freestream velocity. The uncertainty quantification in CFD simulations of the current study was performed for a particular test case and capsule geometry selected from the work of MacLean et al. [2].

Other previous studies regarding uncertainty quantification in different hypersonic re-entry problems include Bose et al. [3], [4], Weaver et al. [5], and Ghaffari et al. [6]. Within these various studies, all input uncertainties were mainly treated as probabilistic. In the current stochastic study to be discussed in the following sections, the freestream velocity was modeled as an inherent uncertain variable described with a probability distribution. The recombination efficiency was modeled as an epistemic uncertain variable, since this uncertainty originates due to the lack of knowledge in a physical model, as described by Oberkampf [7], and represented as an interval with specified bounds. For the quantification of mixed (the aleatory-epistemic) uncertainty, Second-Order Probability Theory was used. [8]−[9] The Point-Collocation

Non-Intrusive Polynomial Chaos (NIPC) Method (Hosder and Walters [10]) was utilized to propagate the input uncertainties in the freestream velocity (inherent uncertainty) and the recombination efficiency (epistemic uncertainty) for the overall quantification of uncertainty in surface heat flux. In general, the NIPC methods which are based on the spectral representation of uncertainty are computationally more efficient than traditional Monte Carlo methods for a moderate number of uncertain variables and can give highly accurate estimates of various uncertainty metrics. In addition, they treat the deterministic model (e.g, the CFD code) as a black box and the uncertainty information in the output is approximated with a polynomial expansion, which is constructed using a number of deterministic solutions each corresponding to a sample point in random space. Therefore, the NIPC methods become a perfect candidate for the uncertainty quantification in the numerical solutions of viscous, non-equilibrium hypersonic flows, which are computationally expensive and complex. More information on the uncertainty quantification in fluid dynamics with NIPC methods can be found in a recent review by Hosder and Walters [11].

1.3. CONTRIBUTIONS OF THE CURRENT STUDY

It is important for any research project to contribute to the "state of the art" in science and engineering from a broad perspective. The current study provides two significant contributions to the topic of design and analysis of complex aerospace vehicles. The first contribution involves implementing and propagating a mixture of aleatory and epistemic uncertainties through a hypersonic flow simulation. The topic of mixed aleatory and epistemic uncertainty quantification in hypersonic flows was not yet investigated before this study. Therefore, the current research project can provide a detailed description on the methods and the overall approach for propagating mixed uncertainties through hypersonic flow simulations for any potential future work on the topic.

The second contribution of this study comes from the particular methodology used to propagate the mixed aleatory-epistemic uncertainties through a "black-box"

simulation code. Second-Order Probability is now a well known method for propagating mixed uncertainties. However, this study modifies the Second-Order Probability method by utilizing a stochastic response surface constructed using NIPC. This response surface is then utilized in the sampling loops of Second-Order Probability as a highly accurate surrogate model for the original "black-box" simulation code. This particular method is much more efficient, when compared to traditional Second-Order Probability, due to the fact that the function evaluation of the stochastic response surface is much less computationally expensive than the original simulation.

1.4. THESIS OUTLINE

This manuscript is composed of six main sections. The second section is a literature review describing relevant work that has been completed on the topic of uncertainty quantification in hypersonic flow and also mixed aleatory and epistemic uncertainty quantification methods. Next, the third section will describe the methodology and approach for aleatory and epistemic uncertainty quantification using Point-Collocation NIPC and Second-Order Probability. Particular attention will be spent on describing the Point-Collocation NIPC and how it can be applied to propagate mixed aleatory-epistemic uncertainties.

The fourth main section of this manuscript describes the implementation of the uncertainty approach to the Fay-Riddell relation for approximating stagnation point heat transfer on a blunt body. Furthermore, the details of the computational procedure involved within the Fay-Riddell calculations will be outlined. Due to the low computational costs of evaluating the Fay-Riddell relation, the results will also be compared to Monte Carlo (MC) simulation results which will assess the validity of the proposed uncertainty quantification approach.

In the fifth main section, all relevant modeling aspects for the high-fidelity CFD simulations will be outlined along with the description of the stochastic nature of the problem at hand. Then the uncertainty results will be presented and sensitivity

analysis will be conducted to describe the relative importance of each uncertainty source. Finally, all relevant conclusions and a discussion on future work will be given in the sixth and final section.

2. LITERATURE REVIEW

The following literature review considers two main topics. The first topic includes a review of previous studies involved with mixed aleatory and epistemic uncertainty quantification. The second topic includes a review of various studies that have been conducted on uncertainty quantification for hypersonic flow applications.

2.1. MIXED UNCERTAINTY QUANTIFICATION

There have been several previous studies conducted on the topic of propagating a mixture of aleatory and epistemic uncertainties through a simulation code. One study, conducted by Eldred et al. [8], provided an extensive summary of efficient algorithms for mixed aleatory-epistemic uncertainty quantification. They proposed using second-order probability for quantifying the effects of mixed input uncertainties. This particular method separates the aleatory and epistemic uncertainties into an inner and outer sampling loop, respectively. By segregating the two sampling loops, it is easy to identify the overall uncertainty which is due to aleatory and epistemic input uncertainties. Furthermore, they also applied the method to a sample problem involving the plastic analysis of a short column which was represented as a simple analytical function. This function represented an ideal test case due to the fact that it was very inexpensive to evaluate. Therefore, this study provided an analytical benchmark for validating in-house codes used for mixed aleatory-epistemic uncertainty quantification. Swiler et al. [12] also performed a similar study which concisely described using second-order probability for mixed uncertainty quantification. They provided several convenient diagrams which were helpful in describing the second order probability method, and also applied the methods to a simple model problem which was intended to be used for code validation.

Guo and Du [13] extended a unified uncertainty analysis framework to reliability analysis for multidisciplinary systems where aleatory and epistemic are present as input uncertainties. They applied their method to a single disciplinary system and then proposed several algorithms to extend the unified reliability analysis framework to multidisciplinary systems. These algorithms were then applied to two different example problems, including a mathematical example and a low-speed aircraft wing design application.

Guo and Du [14] also investigated sensitivity analysis in reliability-based design and analysis involving mixed aleatory and epistemic input variables. They introduced four new types of sensitivity indices for epistemic variables and two new indices for aleatory variables. These indices were calculated using their unified reliability analysis framework along with first order reliability method. An important aspect of this work was that the sensitivity indices were produced as a result of the reliability analysis alone, and there was no need for additional function evaluations. It was also important that the presence of aleatory and epistemic input uncertainties could be handled simultaneously using the proposed reliability analysis. They apply their method to two example problems, where the first example problem involved aleatory variables which had only normal distributions. The second example had aleatory uncertain variables with both normal and non-normal distributions. The epistemic variables were represented using intervals. In both example problems, the sensitivities were given for both the aleatory and epistemic input uncertainties.

Du et al. [15] also studied reliability-based design with a mixture of aleatory and epistemic variables present as input uncertainties. They proposed a method for handling a mixture of aleatory and epistemic input uncertainties by considering the reliability under the "worst case" combination of the epistemic variables. Furthermore, they introduced an efficient approach for the reliability-based design process involving mixed input uncertainties such that the entire analysis was not more computationally expensive than the reliability based-analysis involving only aleatory input uncertainties.

Karanki et al. used a probability bounds (PB) approach for probabilistic safety assessment for industrial installation applications. [16] PB analysis unites traditional probability theory (aleatory uncertainty) and interval arithmetic (epistemic uncertainty) to construct probability boxes (p-boxes) which can be propagated through a simulation.

Jakeman et al. introduced a framework to numerically quantify uncertainties. [17] Their framework attempts to solve an "encapsulation problem" and is capable of varying the amount of known information for the input uncertainties from interval bounds (entirely epistemic) to fully probabilistic (entirely aleatory). Therefore, the framework is capable of handling problems with aleatory uncertainties, epistemic uncertainties, or a mixture of both types of uncertainties.

Eldred also provides a description of Second-Order Probability for quantifying mixed aleatory and epistemic uncertainties using an optimization-based interval estimation technique for calculating the upper and lower bounds of some output metric of interest. [18] He also provides several useful examples with numerical results which can be used for validating uncertainty quantification codes.

As previously mentioned in the Introduction section, the methods used within these studies were applied to various example problems but none of which pertained to hypersonic flow applications. One of the main goals of this study was to implement the mixed aleatory and epistemic uncertainty quantification methods to a hypersonic flow application. In particular, the methods were applied in order to quantify the uncertainty in heat transfer to a hypersonic reentry vehicle [19]. Furthermore, the

current study takes a slightly different approach for uncertainty quantification of mixed epistemic and aleatory input uncertainties by constructing a response surface using the NIPC method.

2.2. HYPERSONIC VEHICLE APPLICATIONS

Various publications have been made on the topic of uncertainty quantification in various hypersonic reentry problems. One study by Bose et al. [3] investigated the uncertainty in aerodynamic heating of a Mars reentry vehicle using high-fidelity computational fluid dynamics (CFD). They also performed sensitivity analysis along with the uncertainty analysis. A Monte Carlo simulation was performed with a total of 130 CFD inputs treated as probabilistic uncertainties. Their main goal was to estimate the contribution of key modeling parameters to the overall uncertainty in the surface heat flux to the reentry vehicle. Another relevant study by Bose et al. [4] investigated the uncertainty and sensitivity analysis in a Titan atmospheric entry problem. Once again, they utilized Monte Carlo for their uncertainty and sensitivity analysis. The main goal of their study was to identify major sources of uncertainty in the various thermochemical models used within the numerical simulation (CFD) and the overall effect it had on the heating to the vehicle during Titan entry.

Another research study was performed by Weaver et al. [5]. Their study was mainly focused on quantifying the uncertainty in surface heat flux to a FIRE-II vehicle during hypersonic reentry due to various probabilistic uncertainties. An important aspect of their study was the implementation of the efficient Polynomial Chaos Gauss-Hermite quadrature method for quantifying the uncertainty. This particular method required much fewer function evaluations to obtain the various statistics on the output variable of interest when compared with traditional sampling methods such as Monte Carlo. Fewer function evaluations made the UQ method much efficient especially when each function evaluation was a costly high-fidelity CFD simulation.

All of these studies have modeled every input uncertainty as probabilistic (aleatory uncertainties). However, there is generally not enough information known regarding

various physical modeling uncertainties involved with hypersonic simulations (e.g. collision integrals). Thus, it is not necessarily appropriate to assign a probability distribution to these uncertain parameters. The current study aims to treat physical modeling uncertainties as interval uncertainties (epistemic) and use efficient methods for propagating them through the numerical simulations.

3. UNCERTAINTY QUANTIFICATION APPROACH

The purpose of this section is mainly to describe in detail the methodology and approach used to propagate uncertainty through general computational simulations. In particular, a novel approach will be described for propagating mixed (aleatory-epistemic) uncertainties in an efficient manner utilizing the NIPC method. It is important to first describe these fundamental methods so that they can be later applied to applications in hypersonic flow, as to be discussed in the following sections.

3.1. UNCERTAINTIES IN COMPUTATIONAL SIMULATIONS

As described in Oberkampf et al. [7], there can be three different types of uncertainty and error in a computational simulation: (1) aleatory uncertainty, (2) epistemic uncertainty, and (3) numerical error. The term aleatory uncertainty describes the inherent variations associated with a physical system. Such variations are due to the random nature of input data and can be mathematically represented by a probability density function (PDF) if substantial experimental data are available for estimating the statistical distribution. Common examples of statistical distribution types are uniform, normal (Gaussian), lognormal, etc. and typical plots for these distributions are shown in Figure 3.1. Selecting appropriate and accurate distribution types for random input parameters is crucial because it can have a drastic impact when propagating the input uncertainty to the uncertainty in the output variable of interest. Aleatory uncertainty is sometimes referred as irreducible uncertainty because the uncertainty will be prevalent in the physical system because of the stochastic behavior of the input parameter. Depending upon the application, there may be numerous sources of aleatory uncertainty within a physical system. The variation of the free

stream velocity or manufacturing tolerances can be given as examples for aleatory uncertainty in a stochastic external aerodynamics problem.

Epistemic uncertainty in a non-deterministic system originates due to ignorance, lack of knowledge, or incomplete information. The key feature of this definition is that the fundamental cause is incomplete information of some characteristics of the system. As a result, an increase in knowledge or information can lead to a decrease in the epistemic uncertainty. Therefore, epistemic uncertainty is referred to as reducible uncertainty. Epistemic uncertainty fundamentally differs from aleatory uncertainty in the sense that epistemic uncertainties can be reduced and aleatory uncertainties cannot be reduced. Another important distinction between aleatory and epistemic uncertainties is that a statistical distribution type cannot be used to describe the nature of the epistemic parameter due to the lack of knowledge or information. As shown by Oberkampf and Helton [20], modeling of epistemic uncertainties with probabilistic approaches may lead to inaccurate predictions in the amount of uncertainty in the responses due to the lack of information on the characterization of uncertainty

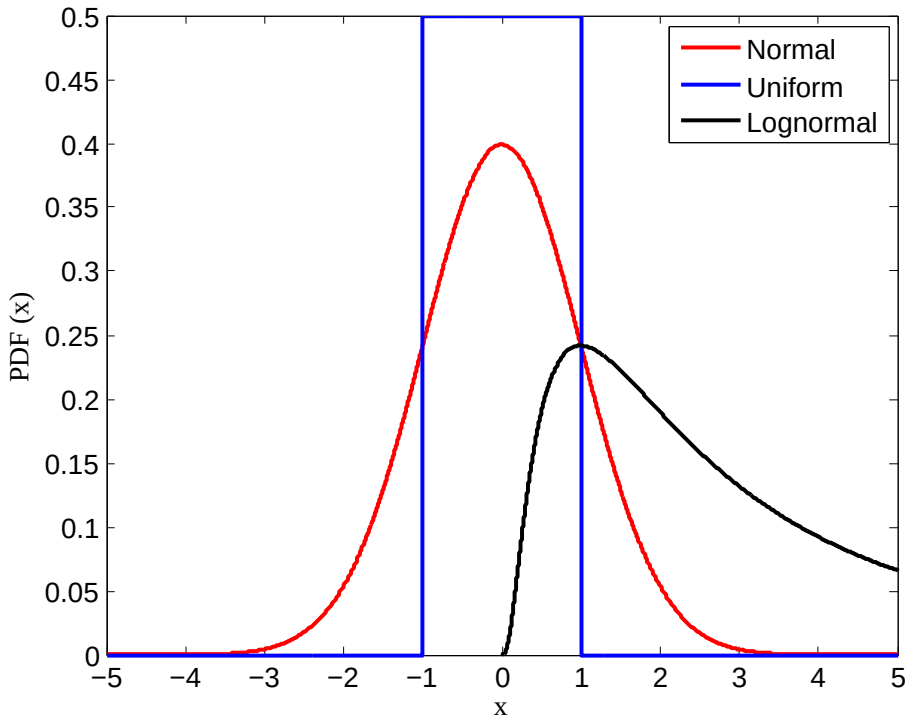

Figure 3.1. Sample probability density functions of common statistical distributions.

as probabilistic. One approach to characterize the epistemic uncertain variables is to use intervals. In this approach, the upper and lower bounds on the uncertain variable can be prescribed using either limited experimental data or expert judgment. All values within this interval are equally likely to occur due to the fact that it is not appropriate to assign a statistical distribution to an epistemic uncertain parameter. Examples of epistemic uncertainties associated with high temperature hypersonic flow simulations can include values of transport quantities, Prandtl number, and catalytic wall recombination efficiencies.

Numerical error is defined as a recognizable deficiency in any phase or activity of modeling and simulation that is not due to the lack of knowledge. If errors cannot be well-characterized, then they must be treated as part of the epistemic uncertainties. The discretization error in spatial or temporal domain originating from the numerical solution of partial differential equations that describes a physical model in a discretized computational space (mesh) can be given as an example of numerical uncertainty. For the perspective of uncertainty quantification, it is very important to minimize the numerical errors associated with computational simulations. Otherwise, the numerical errors can propagate through the simulation along with the given epistemic and aleatory uncertainties and it becomes very hard to decipher the relative contributions to the overall uncertainty in the output variable of interest that is due to input uncertainty or numerical errors.

3.2. MIXED UNCERTAINTY PROPAGATION

It is common to have multiple types of uncertainty associated with a complex simulation such as hypersonic CFD. These types of problems can have a large amount of input parameters and so there can be several sources of aleatory and epistemic uncertainties. It is thus important to account for all of these uncertainties to acquire accurate predictions of the uncertainty in the output of the simulation. In recent years, there has been a great deal of work in developing methods for propagating aleatory and epistemic uncertainties through a black-box simulation code. Several

common methods for propagating pure epistemic uncertainties include possibility theory and fuzzy set theory. However, the particular applications investigated in this study include a mixture of aleatory and epistemic uncertainties. Therefore, another method is needed which is capable of propagating the mixed uncertainties through a simulation code.

3.2.1. Second-Order Probability. In the current study, Second-Order Probability [8]−[9] was utilized to propagate mixed (aleatory and epistemic) uncertainty through several applications such as CFD simulations and the Fay-Riddell model problem. Second-Order Probability uses an inner loop and an outer sampling loop as described in Figure 3.2. In the outer loop, a specific value for the epistemic variable is prescribed and then passed down to the inner loop. Any traditional aleatory uncertainty method may then be used to perform aleatory uncertainty analysis in the inner loop for the specified value of the epistemic uncertain variable. The Second-Order Probability will give interval bounds for the output variable of interest at different probability levels. Each iteration of the outer loop will produce a cumulative distribution function (CDF) based on the aleatory uncertainty analysis in the inner loop. Thus, if there are 100 samples in the outer loop, then 100 different CDF curves will be generated. One major advantage of Second-Order Probability is that it is easy to separate and identify the aleatory and epistemic uncertainties. On the other hand, the two sampling loops can make this method computationally expensive especially if traditional sampling techniques, such as Monte Carlo, are used for the uncertainty propagation.

Since this study is mainly focused on efficient uncertainty propagation, the Point-Collocation NIPC method will be utilized to fit a stochastic response surface to the output quantity of interest (e.g., surface heat flux) as a function of both aleatory and epistemic uncertain variables. The Second-Order Probability approach will then be implemented by outer sampling for the epistemic uncertain variable and the inner sampling for the aleatory uncertain variable (for a fixed value of epistemic uncertain variable) both using the stochastic response surface approximation.

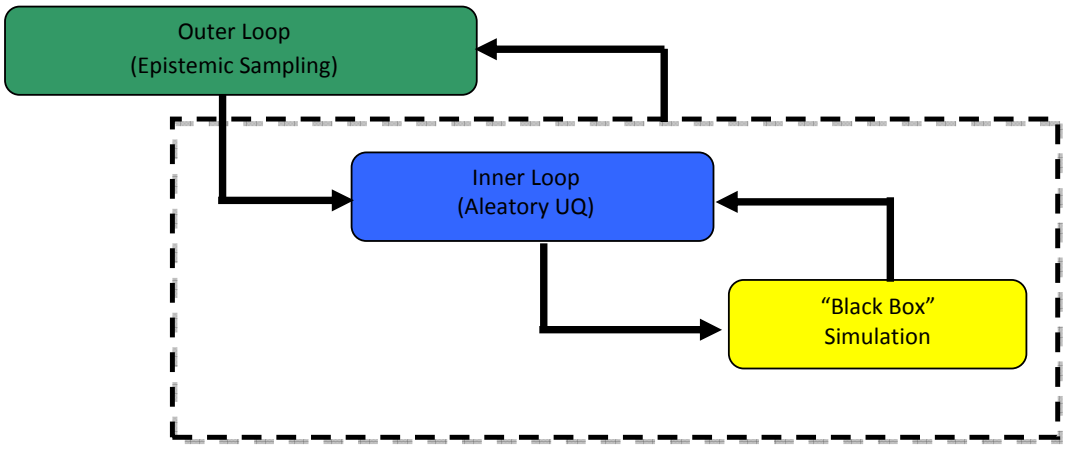

Figure 3.2. Schematic of second-order probability.

3.2.2. Basics of Polynomial Chaos. The Point-Collocation Non-Intrusive Polynomial Chaos is derived from polynomial chaos theory, which is based on the spectral representation of the uncertainty. An important aspect of spectral representation of uncertainty is that one may decompose a random function (or variable) into separable deterministic and stochastic components. For example, for any random variable (i.e., α^*) such as velocity, pressure, or temperature in a stochastic fluid dynamics problem, one can write,

$$\alpha^*(\vec{x},\vec{\xi}) \approx \sum_{j=0}^{P} \alpha_j(\vec{x})\Psi_j(\vec{\xi}) \tag{1}$$

where $\alpha_j(\vec{x})$ is the deterministic component and $\Psi_j(\vec{\xi})$ is the random basis function corresponding to the j^{th} mode. Here we assume α^* to be a function of the deterministic independent variable vector $\vec{x}$ and the n-dimensional random variable vector $\vec{\xi} = (\xi_1, ..., \xi_n)$, which has a specific probability distribution. In theory, the polynomial chaos expansion given by Equation 1 should include infinite number of terms, however in practice a discrete sum is taken over a number of output modes. For a total order expansion, the number of output modes is given by,

$$N_t = P + 1 = \frac{(n+p)!}{n!p!} \tag{2}$$

Table 3.1. Density and weight functions associated with several commonly used univariate optimal bases functions.

Input Distribution	Density Function	Polynomial Name	Weight Function $p(\xi)$	Support Range (R)
Normal	$\frac{1}{\sqrt{2\pi}}e^{\frac{-\xi^2}{2}}$	Hermite $H_n(\xi)$	$e^{\frac{-\xi^2}{2}}$	$[-\infty,\infty]$
Uniform	$\frac{1}{2}$	Legendre $Le_n(\xi)$	1	$[-1,1]$
Exponential	$e^{-\xi^2}$	Laguerre $La_n(\xi)$	$e^{-\xi}$	$[0,\infty]$

which is a function of the order of polynomial chaos (p) and the number of random dimensions (n). The basis function ideally takes the form of multi-dimensional Hermite Polynomial to span the n-dimensional random space when the input uncertainty is Gaussian (unbounded), which was first used by Wiener [21] in his original work of polynomial chaos. To extend the application of the polynomial chaos theory to the propagation of continuous non-normal input uncertainty distributions, Xiu and Karniadakis [22] used a set of polynomials known as the Askey scheme to obtain the "Wiener-Askey Generalized Polynomial Chaos". Table 3.1 displays the weight and density functions for several of the most common polynomials including Hermite, Legendre, and Laguerre polynomials. Huyse et al. [23] have shown that the Hermite, Legendre, and Laguerre polynomials are the optimal basis functions, in terms of the convergence of the statistics, for input uncertainties having Gaussian, uniform, and exponential distributions, respectively. The optimal basis functions are derived based upon the inner product of the weighting functions that correspond to the standard probability density functions (PDF) of a given input uncertainty. A standard PDF must meet the requirement that the integral of the PDF over the support range is exactly one. The constant multiplicative factor between the weight function and density function in Table 3.1 is a direct result of this requirement.

Eldred et al. [24] describes the process of how the multivariate basis functions can be obtained from the product of univariate orthogonal polynomials. For example, a multivariate Hermite polynomial can be constructed using,

$$H_n\left(\xi_{i_1},\ldots,\xi_{i_n}\right) = H_n(\vec{\xi}) = e^{\frac{1}{2}\vec{\xi}^T\vec{\xi}}(-1)^n \frac{\delta^n}{\delta\xi_{i_1},\ldots,\delta\xi_{i_n}} e^{-\frac{1}{2}\vec{\xi}^T\vec{\xi}} \tag{3}$$

which can also be obtained using one-dimensional Hermite Polynomials ($\psi_{m_i^j}(\xi_i)$) by using the multi-index m_i^j, as shown in Equation (4).

$$H_n\left(\xi_{i_1},\ldots,\xi_{i_n}\right) = \Psi_j(\vec{\xi}) = \prod_{i=1}^{n} \psi_{m_i^j}(\xi_i) \tag{4}$$

The main objective of the polynomial chaos method is to determine each of the $\alpha_j(\vec{x})$ coefficients from Equation (1). The statistics of the stochastic output can then be calculated using these coefficients and the optimal basis functions. For example, Hosder et al. [11] show that the mean of a stochastic solution is given by,

$$\mu_{\alpha^*} = \bar{\alpha}^*(\vec{x}) = E_{PC}\left(\alpha^*(\vec{x},\vec{\xi})\right) = \int_R \alpha^*(\vec{x},\vec{\xi})p(\vec{\xi})d\vec{\xi} = \alpha_0(\vec{x}) \tag{5}$$

which demonstrates that the mean, or expected value, of the output $\alpha^*(\vec{x},\vec{\xi})$ is simply the zeroth coefficient (or mode). Hosder et al. [11] also list the result for the variance of the distribution:

$$\sigma^2_{\alpha^*} = Var_{PC}\left[\alpha^*(\vec{x},\vec{\xi})\right] = \int_R \left(\alpha^*(\vec{x},\vec{\xi}) - \bar{\alpha}_0^*(\vec{x})\right)^2 p(\vec{\xi})d\vec{\xi} = \sum_{j=1}^{P}\left[\alpha_j^2(\vec{x}) < \Psi_j^2 >\right] \tag{6}$$

Equations (5) and (6) utilize the fact that $\langle\Psi_j\rangle = 0$ for $j > 0$ and $\langle\Psi_i\Psi_j\rangle = \left\langle\Psi_j^2\right\rangle\delta_{ij}$, where δ_{ij} is the Kronecker delta function. Furthermore, the inner product of $\Psi_i(\vec{\xi})$ and $\Psi_j(\vec{\xi})$ is defined as:

$$\left\langle\Psi_i(\vec{\xi})\Psi_j(\vec{\xi})\right\rangle = \int_R \Psi_i(\vec{\xi})\Psi_j(\vec{\xi})p(\vec{\xi})d\vec{\xi} \tag{7}$$

If the probability distribution of each random variable is different, then the optimal multivariate basis functions can again be obtained using Equation (4) by employing the optimal univariate polynomial at each random dimension. This approach requires that the input uncertainties are independent standard random variables, which also allows the calculation of the multivariate weight functions by the product of univariate weight functions associated with the probability distribution at each random dimension. The detailed information on polynomial chaos expansions can be found in Walters and Huyse, [25] Najm, [26] and Hosder and Walters. [11]

To model the uncertainty propagation in computational simulations via polynomial chaos with the intrusive approach, all dependent variables and random parameters in the governing equations are replaced with their polynomial chaos expansions. Taking the inner product of the equations, (or projecting each equation onto jth basis) yields $P+1$ times the number of deterministic equations which can be solved by the same numerical methods applied to the original deterministic system. Although straightforward in theory, an intrusive formulation for complex problems can be relatively difficult, expensive, and time consuming to implement. To overcome such inconveniences associated with the intrusive approach, non-intrusive polynomial chaos formulations have been considered for uncertainty propagation.

The non-intrusive approach polynomial chaos (NIPC) approach, for approximating $\alpha_j(\vec{x})$ coefficients from Equation (1), is based on spectral projection where $\alpha^*(\vec{x},\vec{\xi})$ is projected onto the k^{th} basis:

$$\left\langle \alpha^*(\vec{x},\vec{\xi}), \Psi_k(\vec{\xi}) \right\rangle = \left\langle \sum_{j=0}^{P} \alpha_j(\vec{x})\Psi_j(\vec{\xi}), \Psi_k(\vec{\xi}) \right\rangle \tag{8}$$

Using the fact that the basis functions are orthogonal,

$$\left\langle \alpha^*(\vec{x},\vec{\xi}), \Psi_k(\vec{\xi}) \right\rangle = \alpha_k(\vec{x}) \left\langle \Psi_k^2(\vec{\xi}) \right\rangle \tag{9}$$

which can then be rearranged as shown in Equation (10). The denominator in Equation (10) can easily be obtained by using the definition of the inner product and

the polynomial basis function. Therefore, the main objective of the spectral projection method is to evaluate the numerator in Equation (10) in order to calculate the polynomial coefficients $\alpha(\vec{x})$. There are four main NIPC methods which include sampling-based, quadrature-based, point-collocation, and stochastic-collocation. The Point-Collocation NIPC was utilized for this study, and it will be described in further detail. Refer to Hosder et al. [11] for more theory regarding the other three NIPC methods.

$$\alpha_k(\vec{x}) = \frac{\left\langle \alpha^*(\vec{x},\vec{\xi}), \Psi_k(\vec{\xi}) \right\rangle}{\left\langle \Psi_k^2(\vec{\xi}) \right\rangle} = \frac{1}{\left\langle \Psi_k^2(\vec{\xi}) \right\rangle} \int_R \alpha^*(\vec{x},\vec{\xi}) \Psi_k(\vec{\xi}) p(\vec{\xi}) d\vec{\xi} \tag{10}$$

3.2.3. Point-Collocation Non-Intrusive Polynomial Chaos. The Point Collocation NIPC method starts with replacing the uncertain variables of interest with their polynomial expansions given by Equation (1). Then, $P+1$ vectors ($\vec{\xi}_i = \{\xi_1, \xi_2, ..., \xi_n\}_k, k = 0, 1, 2, ..., P$) are chosen in random space for a given PC expansion with $P+1$ modes and the deterministic code is evaluated at these points. With the left hand side of Equation (1) known from the solutions of deterministic evaluations at the chosen random points, a linear system of equations can be obtained:

$$\begin{pmatrix} \Psi_0(\vec{\xi_0}) & \Psi_1(\vec{\xi_0}) & \cdots & \Psi_P(\vec{\xi_0}) \\ \\ \Psi_0(\vec{\xi_1}) & \Psi_1(\vec{\xi_1}) & \cdots & \Psi_P(\vec{\xi_1}) \\ \vdots & \vdots & \ddots & \vdots \\ \Psi_0(\vec{\xi_P}) & \Psi_1(\vec{\xi_P}) & \cdots & \Psi_P(\vec{\xi_P}) \end{pmatrix} \begin{pmatrix} \alpha_0(\vec{x}) \\ \\ \alpha_1(\vec{x}) \\ \vdots \\ \alpha_P(\vec{x}) \end{pmatrix} = \begin{pmatrix} \alpha^*(\vec{x},\vec{\xi_0}) \\ \\ \alpha^*(\vec{x},\vec{\xi_1}) \\ \vdots \\ \alpha^*(\vec{x},\vec{\xi_P}) \end{pmatrix} \tag{11}$$

The spectral modes (α_k) of the random variable are obtained by solving the linear system of equations given above. Using these spectral modes, various statistical

information for the output variable of interest can be computed, such as the mean (μ_{α^*}) from Equation (5),

$$\mu_{\alpha^*} = \bar{\alpha}_0(\vec{x}) \tag{12}$$

and the variance ($\sigma^2_{\alpha^*}$) from Equation (6),

$$\sigma^2_{\alpha^*}(\vec{x}) = \sum_{i=1}^{P} \alpha_i^2(\vec{x}) \left\langle \Psi_i^2(\vec{\xi}) \right\rangle \tag{13}$$

as shown by Hosder et al. [10] The solution of the linear problem given by Equation (11) requires $P + 1$ deterministic function evaluations. If more than $P + 1$ samples are chosen, then the over-determined system of equations can be solved using the Least Squares approach. Hosder et al. [27] investigated this option on model stochastic problems by increasing the number of collocation points in a systematic way through the introduction of a parameter n_p (oversampling ratio) defined as the number of samples divided by $P + 1$. They found the optimum n_p to be two. The Point-Collocation NIPC has the advantage of flexibility on the selection of collocation points and possible re-use of collocation points for higher-order polynomial construction (i.e., selection of collocation points with incremental Latin Hypercube sampling). With the proper selection of collocation points, it has been shown that Point Collocation NIPC can produce highly accurate stochastic response surfaces with computational efficiency [27].

3.2.4. Implementation of NIPC in Second-Order Probability. The current study utilizes an efficient approach for the propagation of mixed uncertainties using the framework based on Second-Order Probability. With this approach, the stochastic response (e.g., the surface heat transfer in the current study) is represented with a polynomial chaos expansion on both epistemic and aleatoric variables. In this study, Point-Collocation NIPC is used to construct the stochastic response surface although other NIPC methods (i.e., quadrature or sampling based) can also be used. The optimal basis functions are used for the aleatoric variables whereas Legendre polynomials are used for the epistemic uncertain variables. It should be noted that

the use of Legendre polynomials should not imply a uniform probability assignment to the epistemic variables. This choice is made due to the bounded nature of epistemic uncertain variables. Once the stochastic response surface is formed, at fixed values of epistemic uncertain variables, the stochastic response values can be evaluated for a large number of samples randomly produced based on the probability distributions of the aleatoric input uncertainties (inner loop of Second-Order Probability). This procedure will produce a single cumulative distribution function. By repeating the inner loop procedure for a large number of epistemic uncertain variables sampled from their corresponding intervals (outer loop of Second-Order Probability), a population of cumulative distribution functions can be obtained which can be used to calculate the bounds of the stochastic response at different probability levels. A flowchart of the entire process of propagating mixed aleatory-epistemic uncertainties is shown in Figure 3.3. Due to the analytical nature (polynomial) of the stochastic response, the described procedure will be computationally efficient, especially compared to the approaches based on direct MC sampling which require a large number of deterministic CFD simulations.

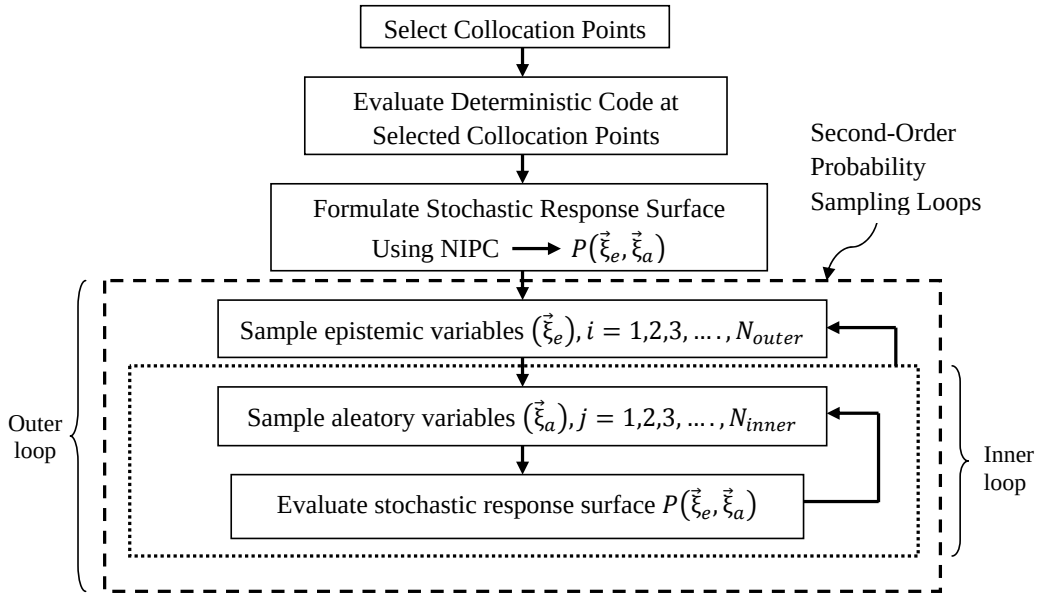

Figure 3.3. Flowchart describing the procedure for propagating mixed aleatory-epistemic uncertainties with Second-Order Probability and NIPC response surface.

4. STOCHASTIC MODEL PROBLEM

4.1. DESCRIPTION OF FAY-RIDDELL CORRELATION

Before initiating the high-fidelity hypersonic CFD problem, the mixed uncertainty quantification approach (the NIPC method and Second-Order Probability) was applied to a model problem which included the prediction of stagnation point heat flux on a blunt body. This particular model problem was relatively inexpensive to evaluate and so it was ideal for validating the uncertainty quantification methods. Stagnation point heat flux was approximated using the Fay-Riddell correlation as described by Fay and Riddell [28]. The Fay-Riddell correlation requires several computational procedures for approximating the stagnation point heat flux such as calculating the properties behind a normal shock wave for equilibrium chemically reacting air and species concentrations for air at a specified temperature and pressure. All procedures and methodology for these computations are outlined in the following sections.

4.1.1. Calculation of Properties Across a Normal Shock Wave. During reentry, the vehicle travels at very high speeds and as a consequence a strong bow shock will develop in front of the vehicle. Shock waves have strong gradients where the flow properties abruptly change across the shock. From a reliability based design point of view, it is important to have a method for accurately calculating properties behind a shock wave. An important observation for this study is that at the stagnation streamline one can assume the bow shock wave to be normal to the flow for axis-symmetric bodies at zero degrees angle of attack. Thus, the normal shock relations can be utilized to calculate properties behind the shock. In general, hypersonic flows will contain strong shocks which can cause the air temperature to be significantly large. At these high temperatures, the air molecules will partially or completely dissociate and thus the traditional calorically perfect gas assumption is no longer valid. In place of the calorically perfect gas, one can assume the air to

be in thermodynamic and chemical equilibrium. For chemical equilibrium, the main assumption is that the time scale of the flow is much smaller than the time scale of the chemical reactions occurring in the flowfield. Also for thermodynamic equilibrium, all internal energy modes are in equilibrium at the translational temperature. Thus, the governing equations (continuity, momentum, and energy) should be utilized assuming equilibrium air (i.e. not calorically perfect). For air in thermodynamic and chemical equilibrium, the procedure for calculating properties behind a normal shock becomes more complex than the traditional calorically perfect gas assumption because a closed form solution is not possible. However, a numerical approach can be implemented to closely approximate the solution for the flow properties behind the shock with a great deal of accuracy. The paragraphs below describe this procedure in detail which is described by Anderson [29].

The first step in the procedure for approximating the properties across a normal shock for equilibrium air is to guess an upper and lower bounds for the density ratio across the shock, as given by the continuity equation in Equation (14) below. In Equation (14), the subscript 1 represents the flow property ahead of the normal shock, and the subscript 2 represents the property behind the shock. A general guideline for guessing the density ratio (ε) is to use 0.0001 and 0.5 as the lower and upper bounds, respectively.

$$\varepsilon = \frac{\rho_1}{\rho_2} = \frac{u_2}{u_1} \tag{14}$$

The next step in the procedure is to calculate the pressure behind the normal shock (P_2) using the initial guess of ε and the momentum equation, as shown in Equation (15).

$$P_2 = P_1 + \rho_1 u_1^2 \left[1 - \varepsilon\right] \tag{15}$$

After the pressure behind the shock has been calculated, the next step is to calculate the enthalpy behind the normal shock (h_2) using the energy equation, as

shown in Equation (16). The enthalpy ahead of the shock (h_1) was calculated using thermodynamic curve fits as described by Srinivasan et al. [30]. A MATLAB code was written for finding the enthalpy as a function of temperature and pressure based on the thermodynamic curve fits by Srinivasan et al. Refer to the code, which is included in Appendix A, for any further details on this procedure.

$$h_2 = h_1 + \frac{u_1^2}{2}\left(1 - \varepsilon^2\right) \tag{16}$$

The fourth step is to calculate the approximate enthalpy behind the normal shock ($\tilde{h}_2$) by again utilizing the thermodynamic curve fits included in the MATLAB code. In Equation (17), the pressure behind the shock (P_{2_i}) was found from Equation (15) and the density behind the shock (ρ_{2_i}) can be calculated using Equation (14).

$$\tilde{h}_2 = \tilde{h}_2\left(P_{2_i}, \rho_{2_i}\right) \tag{17}$$

If a good estimate was made for the density ratio (ε), then the results for $\tilde{h}_2$ and h_2 should be consistent. The difference between $\tilde{h}_2$ and h_2 should meet a desired level of accuracy or tolerance level. A tolerance level of 10^{-6} was selected for this study.

$$\frac{\left|\tilde{h}_2 - h_2\right|}{h_2} < 10^{-6} \tag{18}$$

However, if the guess for ε was not sufficiently accurate (Equation (18) not satisfied), then a new value for ε must be produced. In the present study, the Secant Method was used to calculate the updated values of ε. The equation for the Secant Method is shown below. In Equation (19), ε_{i-1} is the initial guess for the lower bound of ε and ε_{i-1} is the initial guess for the upper bound. Therefore, if the convergence criteria specified in Equation (18) is not satisfied, Equation (19) should be used to calculate an updated value for the ε (guess for the density ratio across the shock). Then, these steps should be repeated until the convergence criteria is satisfied.

$$\varepsilon_{i+1} = \varepsilon_i - \frac{f(\varepsilon_i)}{\frac{f(\varepsilon_i) - f(\varepsilon_{i-1})}{\varepsilon_i - \varepsilon_{i-1}}} \tag{19}$$

where,

$$f(\varepsilon_i) = \tilde{h}_2(\varepsilon_i) - h_2(\varepsilon_i) \tag{20}$$

The overall procedure will produce flow values behind the normal shock wave accurate to the level specified by the convergence criteria. This procedure is essential for the Fay-Riddel model problem, as will be seen in the following sections.

4.1.2. Mass Fraction Calculation for Air. During reentry flight, a reentry vehicle traveling at a very high velocity will experience extreme temperatures. At standard room temperature, air is composed of approximately 20% oxygen (O_2) and 80% nitrogen (N_2) molecules with other trace amounts of molecules such as argon (Ar). However, the molecules will start to dissociate as the temperature of the air increases. At atmospheric pressure, Oxygen molecules begin to dissociate at approximately 2,500 K (Anderson [29]). At a temperature of 4,000 K, almost all Oxygen molecules are dissociated and Nitrogen molecules begin to dissociate. Nitrogen molecules are almost completely dissociated at approximately 9,000 K, and

ionization occurs for even higher temperatures. Some of the important chemical reactions are shown below, where M is a generic third-body.

$$O_2 + M \rightleftharpoons 2O + M \tag{21}$$

$$N_2 + M \rightleftharpoons 2N + M \tag{22}$$

$$N_2 + O_2 \rightleftharpoons 2NO \tag{23}$$

$$NO + M \rightleftharpoons N + O + M \tag{24}$$

$$O_2 + N \rightleftharpoons NO + O \tag{25}$$

$$N_2 + O \rightleftharpoons NO + N \tag{26}$$

The chemical composition (mass fractions) of the air molecules can vary as a function of temperature. This directly affects the heat transfer rate between the air and the structure of the reentry vehicle. Therefore, it is important to take account for this hypersonic phenomena when calculating the heat transfer rate to the vehicle. For this study, the air was assumed to be in chemical equilibrium and a five species model was selected which consisted of O_2, N_2, NO, O, and N (neglecting trace elements). The procedure for calculating the mass fraction of air as a function of temperature and pressure will be described below.

The equilibrium constant is an important parameter which governs the equilibrium composition of air. Statistical thermodynamics and quantum mechanics theory was used to compute the equilibrium constant as a function of temperature as shown by Vincenti and Kruger [31]. A brief outline of this procedure is given in Appendix B. By definition, the equilibrium constant for an atomic specie can also be written

in terms of the partial pressure of each species as shown in Equation (27). The notation a and aa represents the partial pressure for the atomic and molecular specie, respectively.

$$K\left(T\right) = \frac{\left(p^{i,a}\right)^2}{p^{i,aa}} \tag{27}$$

For the five species model selected in this study (O_2, N_2, NO, O, and N), there will be a total of three equilibrium constants. The partial pressure of each species (P_{O_2}, P_{N_2}, P_{NO}, P_O, and P_N) must be solved for, and therefore a total of five equations must be utilized to solve for the five unknowns. The equilibrium constant equations constitute three of the five equations which are necessary. The fourth equation comes from Dalton's Law of partial pressure (Vincenti and Kruger [31]).

$$P = P_{N_2} + P_{O_2} + P_{NO} + P_O + P_N \tag{28}$$

The fifth and final equation comes from the fact that all atoms must be conserved during a chemical process, which essentially implies that no atoms can be created or destroyed during a chemical reaction process. Furthermore, notice that only O and N elements are present in the five-species model for air. Therefore, the atom conservation equation can be written as the following.

$$\frac{\tilde{N}_N}{\tilde{N}_O} = \frac{2P_{N_2} + P_N + P_{NO}}{2P_{O_2} + P_O + P_{NO}} \tag{29}$$

Equation (29) states that the number of moles of Nitrogen (numerator) and Oxygen (denominator) must be equivalent before and after the chemical reaction. Therefore, the five necessary equations are now known from the equilibrium constants, Dalton's Law of Partial Pressure, and atom conservation. For clarity, the exact equations are written below for the five-species model for air.

$$N_2 \rightleftharpoons 2N \qquad \Longrightarrow \qquad K_{N_2}\left(T\right) = \frac{\left(p_N\right)^2}{p_{N_2}} \tag{30}$$

$$O_2 \rightleftharpoons 2O \qquad \Longrightarrow \qquad K_{O_2}(T) = \frac{(p_O)^2}{p_{O_2}} \tag{31}$$

$$NO \rightleftharpoons N + O \qquad \Longrightarrow \qquad K_{NO}(T) = \frac{(p_N p_O)^2}{p_{NO}} \tag{32}$$

$$P = P_{N_2} + P_{O_2} + P_{NO} + P_O + P_N \tag{33}$$

$$\frac{\tilde{N}_N}{\tilde{N}_O} = \frac{2P_{N_2} + P_N + P_{NO}}{2P_{O_2} + P_O + P_{NO}} \tag{34}$$

Notice that Equations (30), (31), (32), (33),and (34) is a system of five non-linear equations. Also note that there are only five unknowns, mainly the partial pressures of of specie. Therefore, this system can be solved using various numerical methods to obtain the desired partial pressures. For this study, a built in function from MATLAB was utilized in solving for the partial pressures. Once the partial pressures are known, the mole fraction can easily be calculated using,

$$X_i = \frac{p_i}{p} \tag{35}$$

where p_i is the partial pressure of the i^{th} specie and p is the pressure behind the normal shock wave. However, the desired quantity is the mass fraction rather than the mole fraction. To convert to mass fraction, one must first find the molecular weight (μ) of the gas mixture behind the normal shock wave using the following:

$$\mu = \sum_{i=1}^{n} X_i \mu_i \tag{36}$$

Finally, the mass fraction can be calculated using Equation (37) below.

$$c_i = X_i \frac{\mu_i}{\mu} \tag{37}$$

For more details regarding the conversion between theory and numerical coding in MATLAB, refer to the source code in Appendix C. The capability of finding the mass fraction of air species behind a normal shock wave as a function of temperature

and pressure will next be directly applied to approximating the stagnation point heat transfer to a hypersonic reentry vehicle.

4.1.3. Fay-Riddell Correlation. The Fay-Riddell correlation was first developed by Fay and Riddell [28] to approximate the stagnation point heat flux to a blunt body. Fay and Riddell first started with the full form of laminar boundary layer equations in a chemically reacting flow. However, the most general form of the equations have no closed-form, exact solution due to the complexity of the equations. So Fay and Riddell restricted the problem to stagnation point flow so that the dependent variables were a function of only one direction. Furthermore, they assumed the flow to be in equilibrium and that the vehicle's wall was fully catalytic. Using these assumptions, Fay and Riddell were able relate the flow variables to the stagnation point heat flux. They were able to reduce the full governing equations down to the following system of equations,

$$\left(l\frac{\partial^2 f}{\partial \eta^2}\right) + f\frac{\partial^2 f}{\partial \eta^2} + \frac{1}{2}\left[\frac{\rho_o}{\rho} - \left(\frac{\partial f}{\partial \eta}\right)^2\right] = 0 \tag{38}$$

$$\frac{\partial\left[\left(\frac{l}{\sigma}\right)(1+d)\frac{\partial g}{\partial \eta}\right]}{\partial \eta} + f\frac{\partial g}{\partial \eta} = 0 \tag{39}$$

where,

$$l \equiv \frac{\rho\mu}{\rho_w\mu_w} = \left(\frac{\alpha_1}{\sqrt{g}}\right) - \left(\frac{\alpha_2}{g}\right) \tag{40}$$

$$\frac{\rho_0}{\rho} = 1 - \gamma_1(1-g) - \gamma_2(1-g)^4 \tag{41}$$

$$d = \beta_1 e^{-\beta_2/g} \tag{42}$$

with boundary conditions,

$$f(0) = 0 \tag{43}$$

$$\frac{\partial f}{\partial \eta}(0) = 0 \tag{44}$$

$$\frac{\partial f}{\partial \eta}(\infty) = 0 \tag{45}$$

$$g(0) = g_0 \tag{46}$$

$$g(\infty) = 1 \tag{47}$$

Equations (38) and (39) are ordinary differential equations subject to the five boundary conditions. Five boundary conditions are necessary because Equation (38) is third order and Equation (39) is second order (i.e. five necessary boundary conditions). Furthermore, the coefficients α_1, α_2, β_1, and β_2 were determined by Fay and Riddell [28] by fitting Equations (40), (41), and (42) to equilibrium air calculations. Thus, Equations (38)- (47) represent a system of differential equations which the solution can be approximated using numerical methods. However, one important thing to note here is that the boundary condition specified in Equations (45) and (47) are specified at the far boundary (∞) rather than at the wall of the vehicle. Therefore, a "shooting-method" numerical technique must be utilized for finding the boundary condition at the wall. This is a fairly simple procedure where a guess is made for the unknown boundary conditions at the wall and the system of equations is solved. Then, the original far boundary condition is compared with the solution of the system of equations to see if they match to a certain tolerance level. If not, then a new guess must be supplied for the wall boundary conditions and this procedure should be repeated until the tolerance level, or level of accuracy, is satisfied. Essentially, this is a root finding problem and so traditional techniques such as Newton's Method can be applied to efficiently determine the boundary conditions at the wall. This process will ultimately produce values for g and f, and these values can be directly related to the heat transfer to the wall of the vehicle. Refer to Fay and Riddell [28] for more details on this relation.

The procedure described above is fairly simple in theory, but it is still somewhat complex to implement into computer code. It is also fairly computationally expensive to solve the system of equations a numerous amount of times. Therefore, Fay and Riddell [28] developed a numerical correlation for the stagnation point heat transfer. This correlation represents an analytical expression which is very consistent with the

solution of the governing equations listed above. Correlations are particularly useful due to their computational efficiency. In other words, the Fay-Riddell correlation is much more computationally efficient than the original system of governing equations and a high level of accuracy is still maintained with the correlation formula. Assuming that the boundary layer was laminar, flow was in equilibrium, and the vehicle's wall was fully catalytic (full recombination at the surface), the final form of the Fay-Riddell correlation ([28] and [29]) which approximates the stagnation point heat transfer to a blunt body is shown below.

$$\dot{q_w} = 0.76\,(Pr)^{-0.6}\,(\rho_w\mu_w)^{0.1}\,(\rho_e\mu_e)^{0.4}\sqrt{\left(\frac{dU_e}{dx}\right)_{sp}}\,(h_{o_e} - h_w)\left[1 + \left(Le^{0.52} - 1\right)\left(\frac{h_D}{h_{o_e}}\right)\right] \tag{48}$$

where

$$\left(\frac{dU_e}{dx}\right)_{sp} = \frac{1}{R_N}\sqrt{2\frac{p_e - p_\infty}{\rho_e}} \tag{49}$$

$$h_D = \sum_i C_{i_e}\,(\Delta h_f)_i^\circ \tag{50}$$

In Equation (48), the Pr symbolizes the Prandtl Number which was assumed to be 0.714 and Le symbolizes the Lewis Number which was taken to be 1.4. The subscripts e and w represent the property at the edge of the boundary layer and at the wall of the vehicle, respectively. Also, R_N represents the radius of the truncated sphere of the spherical capsule which was obtained from the experimental set-up described by MacLean et al. [2]. In Equation (50), C_i represents the species mass fraction behind the normal shock wave which was calculated using statistical thermodynamics [31], as described previously. In these calculations, the heats of formation at absolute zero, $(\Delta h_f)_i^\circ$, were taken as zero for the molecules. The properties behind the normal shock were found with equilibrium air assumption using thermodynamic curve fits by Srinivasan et al. [30]. The freestream conditions correspond to one of the experimental test cases conducted by MacLean et al. [2] (Table 4.1) and the wall temperature was

held constant at 300 K (cold-wall boundary condition), which was consistent with the experiment. It should be noted that the conditions of the experimental test case were used just as reference values for the model problem and not for comparison, since the actual flow in the tests are in thermo-chemical non-equilibrium.

4.2. DESCRIPTION OF THE STOCHASTIC PROBLEM

The freestream velocity and the dynamic viscosity at the boundary layer edge (μ_e) were treated as random variables within the Fay-Riddell relation. The freestream velocity was assumed to be an inherent uncertain variable and the coefficient of viscosity (physical model parameter) was assumed to be an epistemic uncertain variable. The dynamic viscosity was modeled using Sutherland's Law. It is known that the accuracy of Sutherland's Law degrades at high temperatures beyond 3000°K due to dissociation and ionization effects. The uncertainty in the dynamic viscosity was demonstrated by Anderson [29], which is shown in Figure 4.1 for clarity. In Figure 4.1, the Sutherland's calculation is normalized by a more accurate calculation of the dynamic viscosity which can be obtained using either high-order models or curve-fits. Notice in the figure that there is quite a large discrepancy between the two calculations as the temperature increases. This demonstrates the importance of accounting for the uncertainty in dynamic viscosity for hypersonic, high temperature, applications.

One can use high-order models or curve-fits to increase the prediction accuracy of viscosity at high temperatures. However, by retaining Sutherland's Law in this

Table 4.1. Table outlining the free stream conditions for the CFD (Case 1) and the model problem (Case 2).

Case #	H_0 (MJ/kg)	V_∞ (m/s)	T (K)	ρ_{N_2} (kg/m^3)	ρ_{O_2} (kg/m^3)	ρ_{NO} (kg/m^3)	ρ_O (kg/m^3)
1	4.7	2922	180	$2.26 \cdot 10^{-3}$	$6.10 \cdot 10^{-4}$	$2.14 \cdot 10^{-4}$	$1.51 \cdot 10^{-6}$
2	9.9	4167	522	$1.17 \cdot 10^{-3}$	$2.72 \cdot 10^{-4}$	$1.04 \cdot 10^{-4}$	$4.60 \cdot 10^{-5}$

study, an epistemic uncertainty was intentionally introduced to the model problem. In specific, the coefficient of viscosity was modeled as an epistemic variable through the introduction of a factor (k) which is multiplied with the value obtained with Sutherland's Law (e.g., $\mu_e = k \times \mu_{e_{ref}}$). This factor is treated as an epistemic uncertain variable with a specified interval which had the upper and lower bounds approximated using the following procedure: First, a stagnation temperature of 4,388°K behind a normal shock wave was obtained with the equilibrium air calculations using the mean freestream velocity, as described in the previous sections. Then, the chart in Figure 4.1 was utilized to approximate the range of variation for the coefficient of viscosity at the calculated temperature relative to the value calculated by the Sutherland's Law. This gave an upper and lower bounds of 1.0 to 1.15 for the multiplier k, which has been used in the calculations.

The freestream velocity was assumed to have a uniform distribution with a mean of 4167 m/s (Run 2), which was the nominal velocity in the test section of the wind tunnel for the experiments from MacLean et al. [2] The lower and upper bounds were set at 3958.65 m/s and 4375.35 m/s, respectively, which corresponds to a $\pm$ 5% percent uncertainty in the freestream velocity. For comparison purposes, the freestream velocity was also modeled as a normal random variable with a mean of

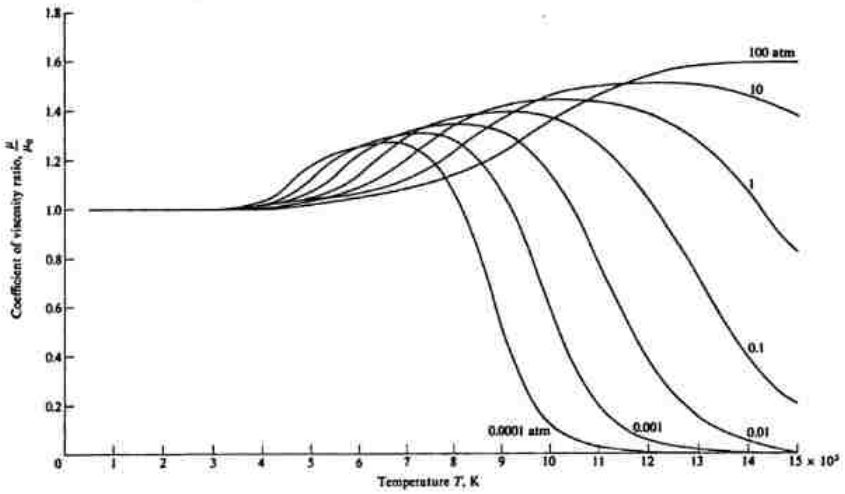

Figure 4.1. Variation of coefficient of viscosity as a function of temperature and pressure (Anderson [29]).

4167 m/s and a standard deviation of 100 m/s. The standard deviation in velocity was selected with the intention of producing consistent standard deviation values for the stagnation heat transfer for both uniform and normal distributions.

4.3. MIXED UNCERTAINTY QUANTIFICATION

The approach described in Section 3 was followed to propagate the mixed (aleatory and epistemic) uncertainty through the Fay-Riddell relation. It is important to realize that the results of the uncertainty propagation approach is dependent upon the polynomial order used within the NIPC method. Furthermore, the number of function evaluations drastically increases with the polynomial order (p). Therefore, it is important to intelligently select an appropriate value for p. An optimal value for p would be a high enough value to produce accurate results while requiring the smallest number of required function evaluations. In order to find the optimal value for p, convergence studies were carried out where the average and standard deviation of the stagnation point heat flux was analyzed as a function of polynomial order. The results are shown in Figures 4.2 and 4.3. From the figures, it is clear that a 3^{rd} order polynomial chaos was sufficient for convergence of the NIPC response surface. This can be seen from the fact that there is no noticeable changes in the average and standard deviation of the stagnation point heat flux for values of p higher than three. Therefore, a third order polynomial was selected along with an over-sampling ratio of two which corresponded to a total of 20 Fay-Riddell function evaluations needed to construct the NIPC response surface. The sample points were selected according to the respective statistical distribution of each stochastic input variable.

After the convergence study had been completed, the next step was to perform the mixed aleatory-epistemic uncertainty propagation techniques to the Fay-Riddell relation. A Latin Hypercube Sample (LHS) of size 5,000 was used for the outer loop (epistemic) sampling for μ. For each value of μ, the NIPC response surface was utilized for the inner-loop (aleatory) UQ which produced a single cumulative distribution function (CDF). The overall Second-Order Probability analysis produced 5,000

CDF curves. Figure 4.4 shows the mixed uncertainty results for uniformly distributed velocity and Figure 4.5 displays the results for velocity modeled with a normal distribution. In each figure, the left plot shows the results obtained with Second-Order Probability approach with the NIPC response surface formulation and the other plot gives the results obtained with a direct Monte Carlo (MC) approach that utilized 10,000 samples for the outer-loop and 5,000 samples for the inner loop (a total number of 5×10^7 Fay-Riddell evaluations). By comparing the results of NIPC and MC, it can clearly be seen that the NIPC results compare well with MC. This indicates that the the stochastic response surface approach to Second-Order Probability is performing well. These results help validate the current method for mixed uncertainty propagation and provides confidence for using the same method in CFD simulations (to be discussed in the next section). Figures 4.4 and 4.5 also imply a fairly linear dependency of stagnation point heat transfer on the statistical distribution type of the freestream velocity. In Figure 4.4, the velocity has a uniform distribution and the CDF shapes show that the distribution of stagnation heat transfer is fairly uniform as well. Similarly for Figure 4.5, the velocity has a Gaussian distribution and the CDF curves for stagnation point heat transfer are very similar to typical Gaussian CDF

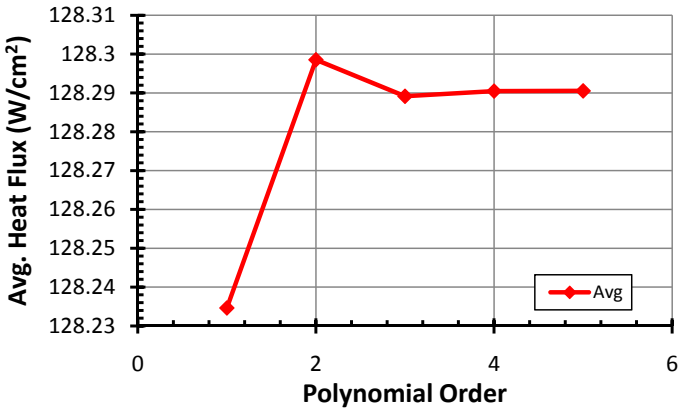

Figure 4.2. Convergence of the average stagnation point heat transfer.

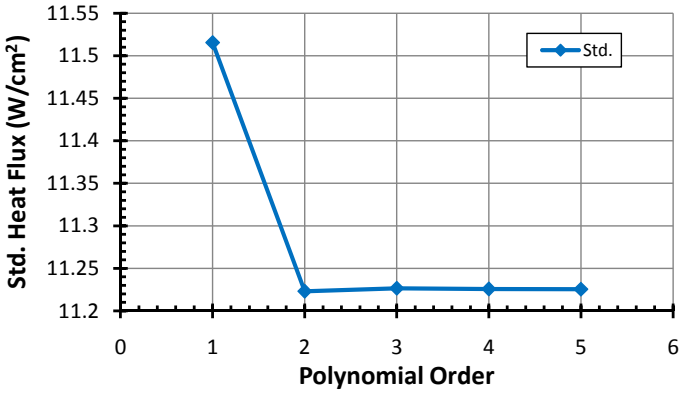

Figure 4.3. Convergence of the standard deviation of stagnation point heat transfer.

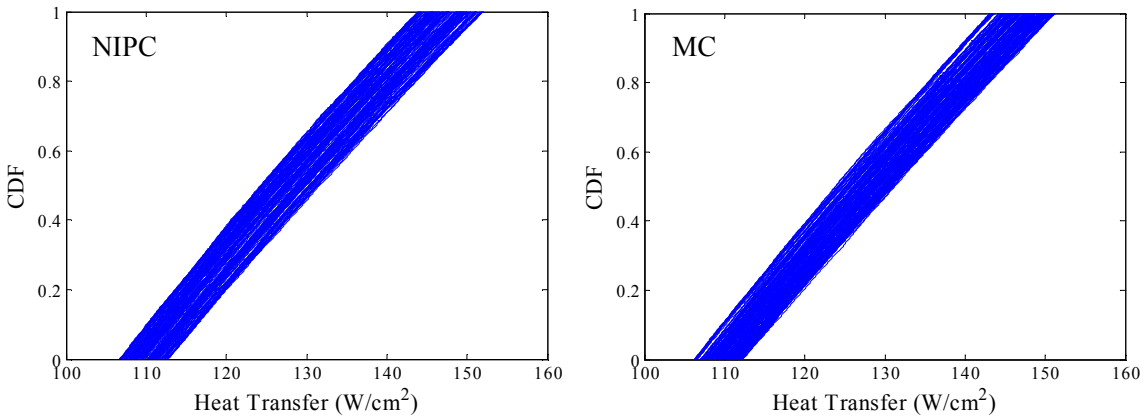

Figure 4.4. Horse-tail plot representing mixed aleatory-epistemic uncertainty results for the Fay-Riddell model problem (uniform distribution for velocity).

curves. These results also demonstrate the importance of distribution type for modeling aleatoric variables. When the distribution type for the velocity was changed from uniform to normal, the results from Second-Order Probability were also significantly altered.

Stagnation heat flux information at particular probability levels are shown in Tables 4.2 and 4.3 which is for the uniform and normal distribution of freestream velocity, respectively. In these tables, the heat flux uncertainty results obtained from Second-Order Probability are reported using intervals at each probability level. The second column in the table is for the results obtained with the NIPC response surface formulation for uncertainty propagation and the third column shows results obtained

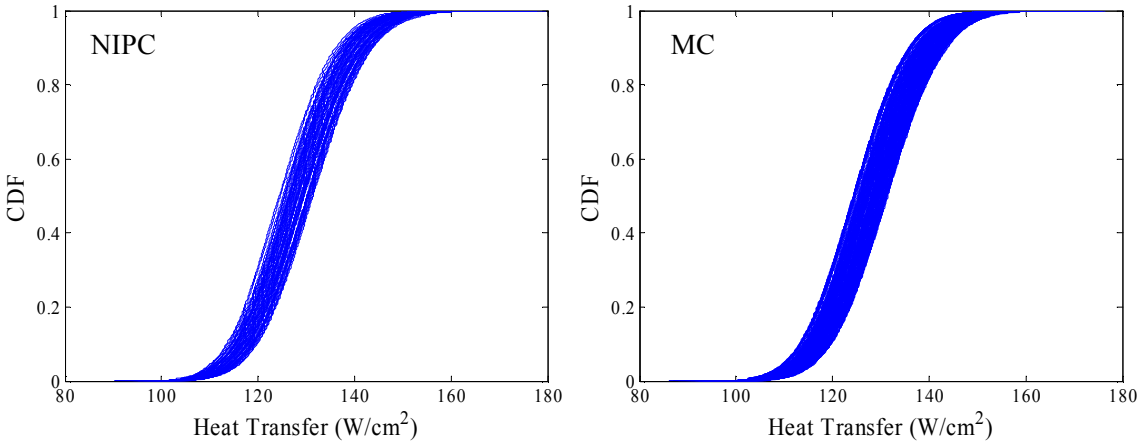

Figure 4.5. Horse-tail plot representing mixed aleatory-epistemic uncertainty results for the Fay-Riddell model problem (normal distribution for velocity).

with the MC. Once again, the NIPC results are consistent with the MC which demonstrates the effectiveness of the NIPC method. The fourth column lists the results from a pure aleatory uncertainty analysis that modeled the coefficient of viscosity as a uniform random variable. The same 3^{rd} order NIPC response surface was used to propagate the aleatory uncertainty. Although it may not be appropriate to treat the coefficient of viscosity as a probabilistic uncertainty due to its nature, the results are shown here for the purpose of comparison to mixed uncertainty results. It can be seen that only a single value is available (not an interval) at each probability level for the aleatory NIPC results.

Table 4.2. Stagnation point heat transfer (W/cm^2) at different probability levels for the model problem (Free-stream velocity is taken as a uniform random variable).

Probability Level	Second-Order Probability (NIPC)	Second-Order Probability (MC)	Aleatory (NIPC)
P = 0.0	[106.67, 112.80]	[106.18, 112.29]	106.86
P = 0.2	[113.25, 120.36]	[112.97, 119.86]	116.92
P = 0.4	[120.23, 128.06]	[120.15, 127.45]	124.32
P = 0.6	[127.62, 135.87]	[127.48, 135.26]	131.91
P = 0.8	[135.37, 144.04]	[135.16, 143.20]	139.89
P = 1.0	[143.86, 152.13]	[143.14, 151.37]	151.94

Table 4.3. Stagnation point heat transfer (W/cm^2) at different probability levels for the model problem (Free-stream velocity is taken as a normal random variable).

Probability Level	2^{nd} Order Probability (NIPC)	2^{nd} Order Probability (MC)	Aleatory (NIPC)
P = 0.0	[81.80, 103.29]	[83.31, 101.73]	90.14
P = 0.2	[116.81, 124.10]	[116.72, 123.78]	120.35
P = 0.4	[121.90, 129.45]	[121.94, 129.21]	125.67
P = 0.6	[126.42, 134.24]	[126.42, 133.91]	130.43
P = 0.8	[131.63, 139.88]	[131.76, 139.61]	136.07
P = 1.0	[154.78, 186.28]	[156.07, 184.57]	168.41

4.4. SENSITIVITY ANALYSIS

The purpose of global sensitivity analysis (SA) is to measure or rate the importance of individual uncertain random variables on the overall uncertainty in an output variable of interest from a simulation code. For the model problem, a global SA approach was used to provide the relative importance of each of the two uncertain variables on the stagnation point heat transfer uncertainty. Helton et al. [32] describes a sampling-based SA procedure using linear regression for calculating correlation coefficients and interpreting the results based on these coefficients. Bose et al.[3, 4] considered a similar SA approach in their uncertainty quantification studies of hypersonic entry into Martian and Titan atmospheres. The same linear global SA method was used in this study by creating a total number of 20,000 samples from the 3^{rd} order stochastic response obtained for the uncertainty analysis described in the previous section.

The SA results are shown in the form of scatter plots in Figures 4.6, 4.7, 4.8, and 4.9. Figures 4.6 and 4.7 shows results for the freestream velocity having a uniform distribution and Figures 4.8 and 4.9 are the results for velocity having a normal distribution. Figures 4.6 and 4.8 shows the stagnation point heat transfer as a func-

tion of freestream velocity and Figures 4.7 and 4.9 displays the stagnation point heat transfer as a function of $k = \mu_e/\mu_{e_{ref}}$. Qualitatively, one can see the relative importance simply by observing the thickness of the band in the scatter plot. It is obvious that the freestream velocity has a more drastic impact on stagnation point heat transfer for the Fay-Riddell model problem. This is consistent for the freestream having both a uniform and normal distribution. Furthermore, the correlation coefficient was calculated using linear regression [32] and is imposed on the plots in Figures 4.6, 4.7, 4.8, and 4.9. The correlation coefficient (CC) gives an indication of the linear relationship between the stochastic inputs and the output variable of interest. A CC value of one indicates a perfect linear relationship between the input uncertainty and the output uncertainty. Notice that the CC is close to one for the velocity. In contrast, the CC for k is approximately 0.2 for both distributions. Thus, by also comparing the correlation coefficients, it is clear that the uncertainty in the freestream velocity contributes more to the overall uncertainty in the stagnation point heat transfer.

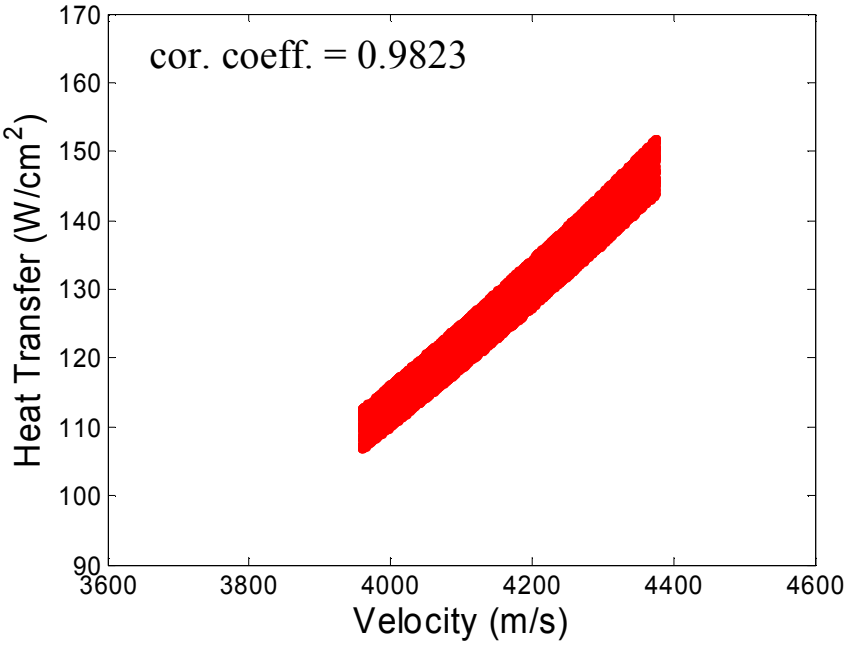

Figure 4.6. Correlation plots demonstrating the influence of velocity on the overall uncertainty in the stagnation heat flux with velocity following a uniform distribution.

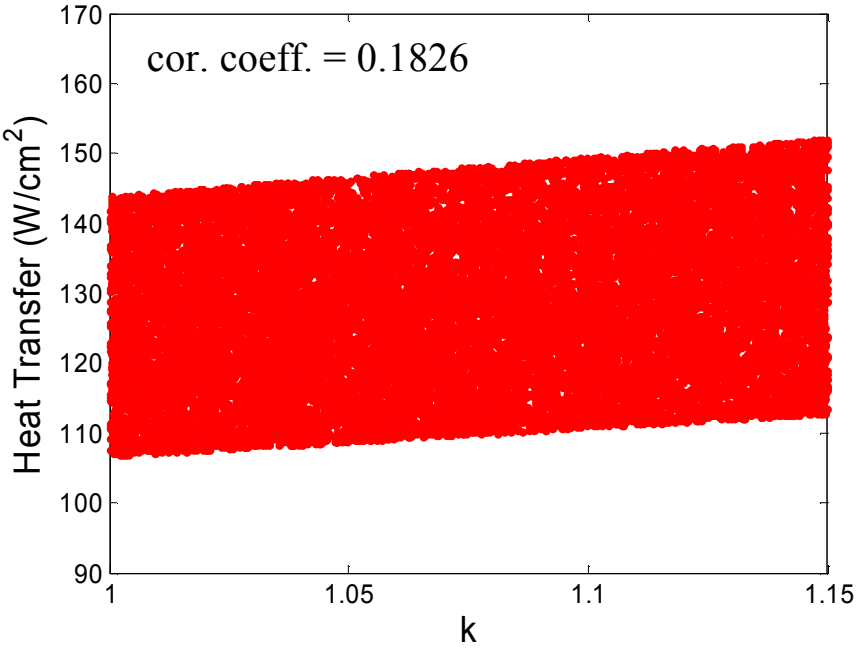

Figure 4.7. Correlation plots demonstrating the influence of k ($k = \mu_e/\mu_{e_{ref}}$) on the overall uncertainty in the stagnation heat flux with velocity following a uniform distribution.

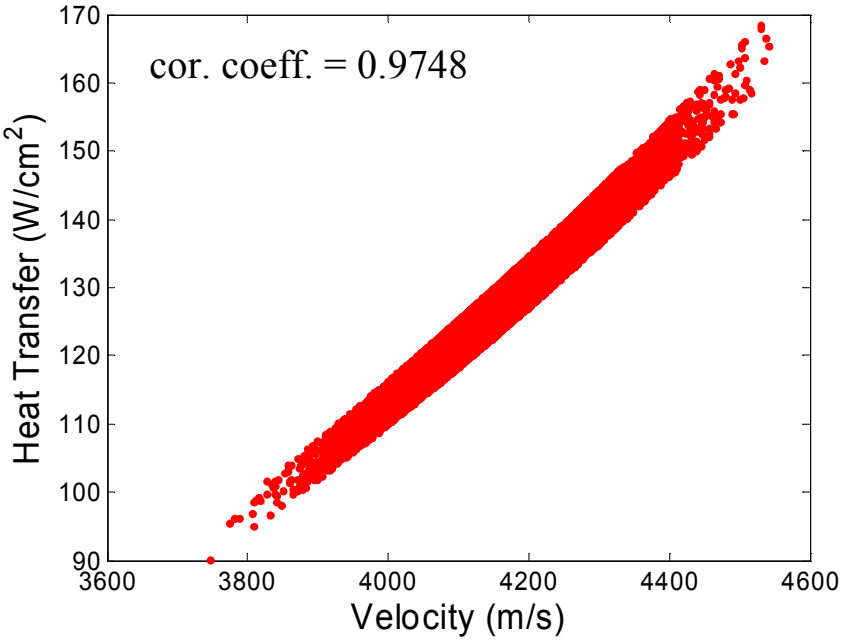

Figure 4.8. Correlation plots demonstrating the influence of velocity on the overall uncertainty in the stagnation heat flux with velocity following a normal distribution.

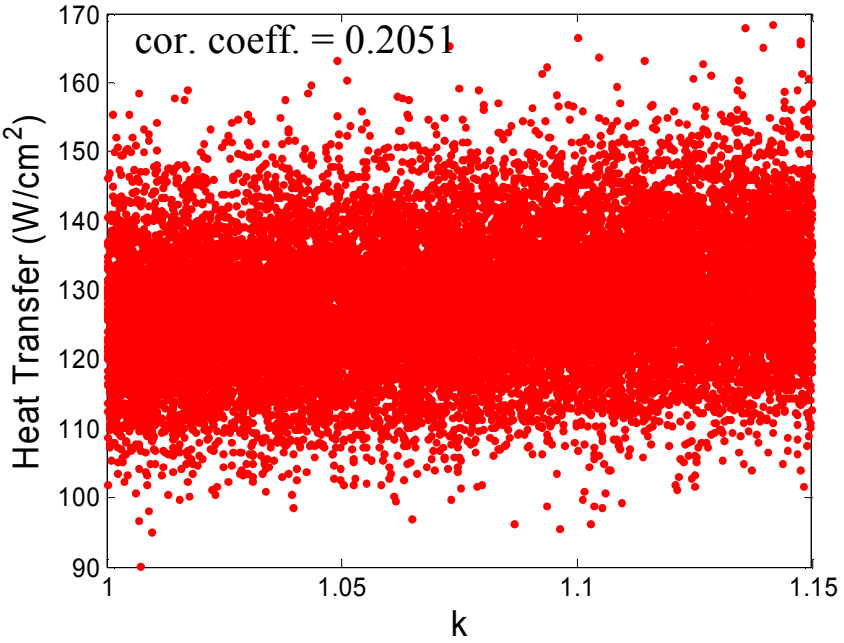

Figure 4.9. Correlation plots demonstrating the influence of k ($k = \mu_e/\mu_{e_{ref}}$) on the overall uncertainty in the stagnation heat flux with velocity following a normal distribution.

5. UNCERTAINTY QUANTIFICATION IN CFD SIMULATIONS

The primary focus of this section is to apply the efficient uncertainty quantification approach described in Section 3 to a high-fidelity CFD simulation in order to quantify the uncertainty in the surface heat flux to the spherical non-ablating heat-shield of a reentry vehicle at zero-angle of attack due to epistemic and aleatory uncertainties that may exist in various models and parameters used within the CFD simulation. The uncertainty quantification was performed for a particular test case and capsule geometry selected from the work of MacLean et al. [2].

5.1. INTRODUCTION TO COMPUTATIONAL FLUID DYNAMICS

Computational fluid dynamics (CFD) is a vital tool in the analysis and design of complex aerospace systems. The main goal of CFD is to provide an accurate representation of fluid flow over an arbitrary geometry, and extract valuable fluid flow variables (temperature, pressure, velocity, etc.) at any point in the entire flowfield. Hypersonic experiments are both difficult and expensive to perform, and so it is important to have an accurate numerical approximation (such as CFD) to replace or supplement these experiments in the design process of a hypersonic vehicle.

To numerically approximate the fluid flow over an given geometry, the governing equations, in the form of highly couples partial differential equations (PDE's), must be discretized. The most general form of fluid dynamic equations are known as Navier-Stokes, and these equations are implemented into most modern CFD codes. Additional equations must also be added for more complex fluid flows such as high temperature, hypersonic, flows which involve thermo-chemical non-equilibrium. A common numerically scheme for approximating the governing equations is the finite volume method, which is utilized in most CFD codes. This particular method requires a computational mesh domain of the geometry of interest and a sufficient amount of volume surrounding the geometry. One may use either a structured or unstructured

computational mesh, depending on the problem at hand or the capabilities of the CFD software. Once a computational mesh has been constructed, one must specify the freestream, or farfield, conditions to be used in the simulation. Furthermore, in any type of process involving the numerical approximation of PDE's, it is crucial to accurately model all relevant boundary conditions for the problem at hand. For example, one may specify the surface of the vehicle to be an adiabatic "no-slip" wall BC for many low speed aerodynamic applications. Furthermore, the user must specify the most appropriate physical models for the problem at hand. For example, if the problem involves hypersonic high-temperature flows, then it is most appropriate to choose a chemical non-equilibrium chemistry model for the fluid. Lastly, the user must specify all relevant methods to be used in the numerical approximation scheme utilized within the CFD code. These may includes things such as inviscid flux modeling, limiters, and parallel computing options.

It is also important to ensure the CFD code produces accurate results. To accomplish this task, one must ensure that the physical modeling errors are kept to a minimum by selecting appropriate models, and also the discretization error should be minimized. Discretization error is directly related to the grid density of the computational mesh used within the CFD. It is a good practice to perform grid convergence studies to ensure that the CFD solution is grid independent and that the discretization error is kept at a minimum. If these steps are followed, then the accuracy of CFD results can be increased for the analysis and design of complex aerospace vehicle and they can be a beneficial supplement to costly wind tunnel experiments.

5.2. COMPUTATIONAL MODELING

5.2.1. CFD Solver and Numerical Scheme. The high-fidelity CFD simulations were performed with GASP [33], a three-dimensional, structured, finite-volume, RANS code which is capable of modeling high-speed flows with frozen, equilibrium, or non-equilibrium thermo-chemistry. For modeling the inviscid fluxes, the

Roe-Harten inviscid flux scheme was utilized with a third order accurate upwind biased MUSCL approach and Min-Mod limiter. The Roe-Harten scheme is particularly useful for high speed blunt body flows because it helps to avoid carbuncle effect near the stagnation region. The CFD simulations were performed using parallel MPI processing on a high-performance Linux computing cluster consisting of 64 processors to help ease computational costs.

5.2.2. Boundary Conditions. A no-slip non-ablating boundary condition was specified at the capsule wall, and the wall temperature was held at 300°K to enforce a cold-wall boundary condition, which is consistent with the experiment. Simulations were conducted at zero degrees angle of attack which allowed an axis-symmetric flow assumption. The freestream was fixed at the values from Case #1 shown in Table 4.1, and a 1^{st} order extrapolation was specified for the outflow.

An important aspect of GASP for this study is the capability of modeling wall recombination efficiencies (γ) for partially catalytic walls. The GASP code utilizes the method described by Milos et al. [1] to model the non-ablating finite rate catalytic wall boundary condition that requires the specification of recombination efficiency (γ) for Nitrogen and Oxygen atoms [34, 35, 36]. For the current study, the catalytic wall represents recombination of dissociated oxygen and nitrogen species on the wall with a certain percentage. The limiting case of a fully-catalytic wall represents complete recombination at the wall (100% efficiency), and the non-catalytic wall represents zero recombination (0% efficiency). In terms of the heat transfer to the vehicle, a fully-catalytic wall provides the highest heat transfer due to the exothermic nature of the recombination process and a non-catalytic wall provides the lowest amount of heat transfer. Thus, fully-catalytic and non-catalytic walls represent the theoretical upper and lower bounds of the heat flux to the vehicle for a given set of flight conditions. The catalytic wall model used in this study does not include the surface reactions that include the recombination of the nitric oxide (NO) species. The heat flux to the surface of the reentry vehicle, at a freestream velocity of 2922 m/s, is shown in Figure 5.1. A significant variation in heat flux to the surface can be seen

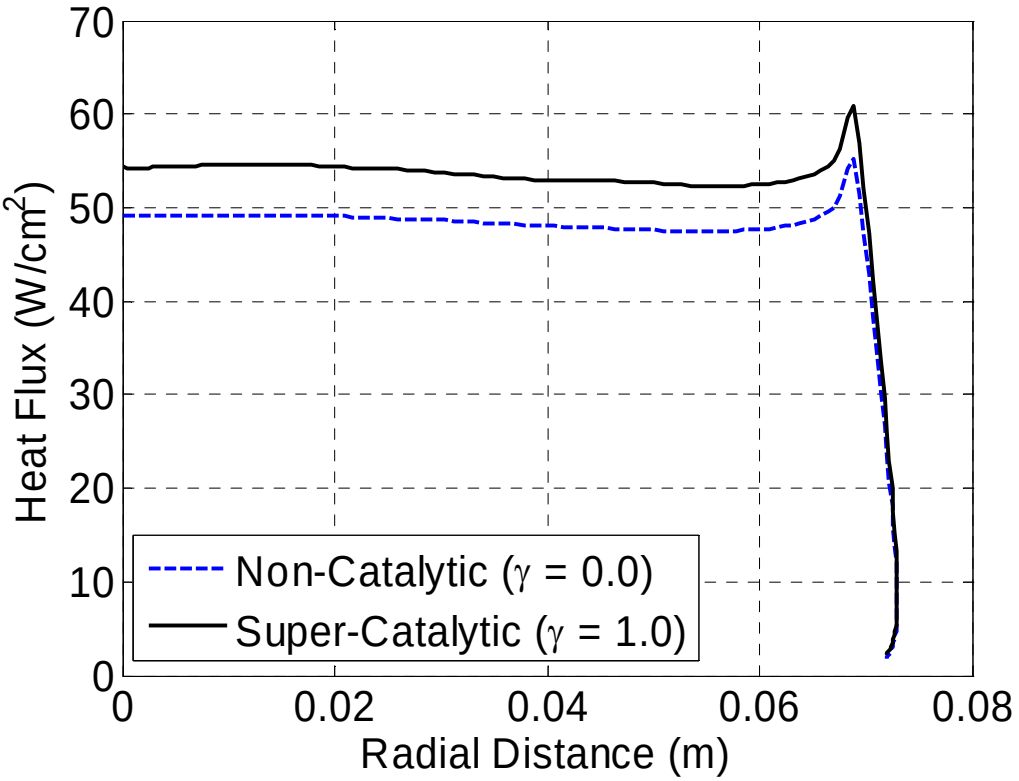

Figure 5.1. CFD solution for surface heating for fully-catalytic and non-catalytic wall boundary condition.

when comparing the non-catalytic (γ=0.0) and fully-catalytic (γ=1.0) wall boundary condition specification which will be the basis of the uncertainty modeling in the following section.

5.2.3. Physics Modeling. In accordance with the experimental test case selected from MacLean et al. [2] which is used in the current stochastic CFD study, laminar flow was assumed for modeling the viscous terms. A five species chemical model, Park [37], is selected for this study in order to model the high temperature air. Also, finite rate chemistry is used to obtain the highest level of accuracy of the chemical reactions that occur behind the shock wave. Furthermore, a vibrational non-equilibrium model was selected with three non-equilibrium energies coming from the diatomic molecules included in the 5-species Park model. Vibrational non-equilibrium rates are modeled using the formulation given by Millikan and White. [38]. The CFD simulations utilized the curve-fits by Gupta et al. [39] for approximating the collision integrals required to calculate the transport quantities (viscosity, diffusion

coefficient, and thermal conductivity) for high temperature non-equilibrium flows. At the particular velocity range considered in this study, the main mechanisms that contribute to the total surface heat flux will be heat conduction to the surface via translational and vibrational modes and the diffusion of chemical energy flux to the surface which will depend on the surface catalysis. The radiation heat transfer is not modeled in the present work.

5.2.4. Computational Grid. The computational grid used for the CFD simulations was provided by Maclean et al. [2]. The original grid dimensions were 257 grid points in the streamwise direction and 229 in the normal direction and the geometry of the vehicle was based upon the experiments performed by MacLean et al. [2] which utilized the capsule geometry shown in Figure 5.2. Grid convergence studies were conducted to find the optimum grid mesh size in terms of minimizing the discretization error and computational expense by dividing the original grid into coarser grid levels by skipping every other grid point in both the normal and stream-wise directions. Additional grid points were added at the outer boundary in the normal direction to obtain converged CFD solutions. Convergence studies demonstrated that the optimum mesh size was 129 grid points in the streamwise direction and 130 in the normal direction and the final grid used for all the CFD simulations is shown in Figure 5.3. Since the CFD runs were conducted for test cases involving the capsule geometry at zero degrees angle of attack, the numerical solutions were obtained with an axis-symmetric flow assumption. The left side of Figure 5.3 is the entire domain of the grid. On the right side of Figure 5.3 is a zoomed in view of the stagnation line in order to help visualize the grid spacing. A sample pressure contour plot is shown in Figure 5.4 to demonstrate that a well converged CFD solution had been obtained with the current computational grid.

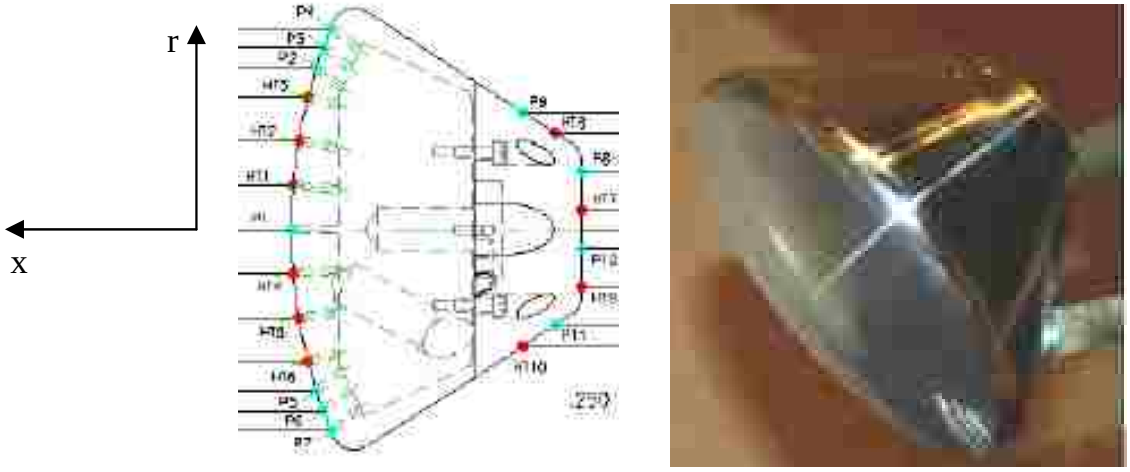

Figure 5.2. Geometry and coordinate nomenclature for the reentry vehicle used in the experiments by MacLean et al. [2]

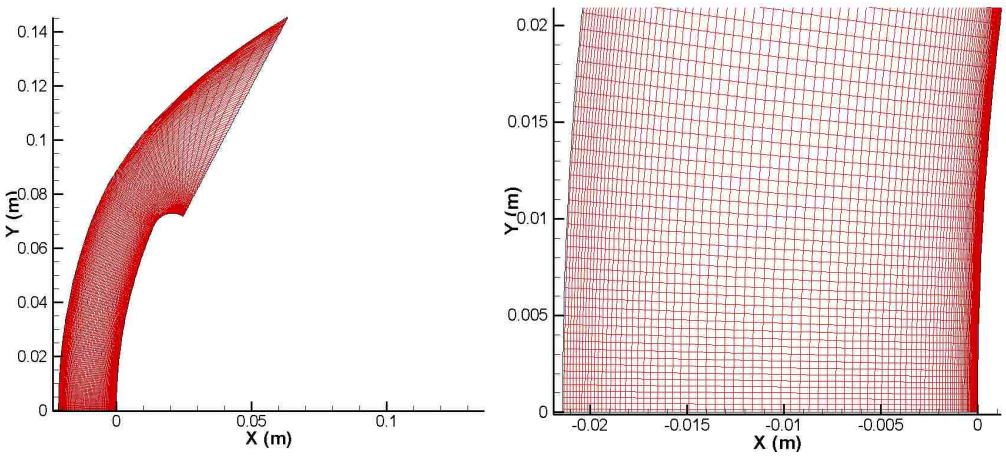

Figure 5.3. Computational grid for the 2-D axis-symmetric spherical capsule.

5.3. DESCRIPTION OF THE STOCHASTIC PROBLEM

In general, it is difficult to obtain the exact values of the recombination efficiencies for different wall materials, temperatures, and gas species, therefore γ is considered as one of the uncertainty sources in this study. Recombination efficiency is mainly a physical modeling parameter so it is appropriate to treat it as an epistemic uncertain variable. In this study, the same recombination efficiency for oxygen and

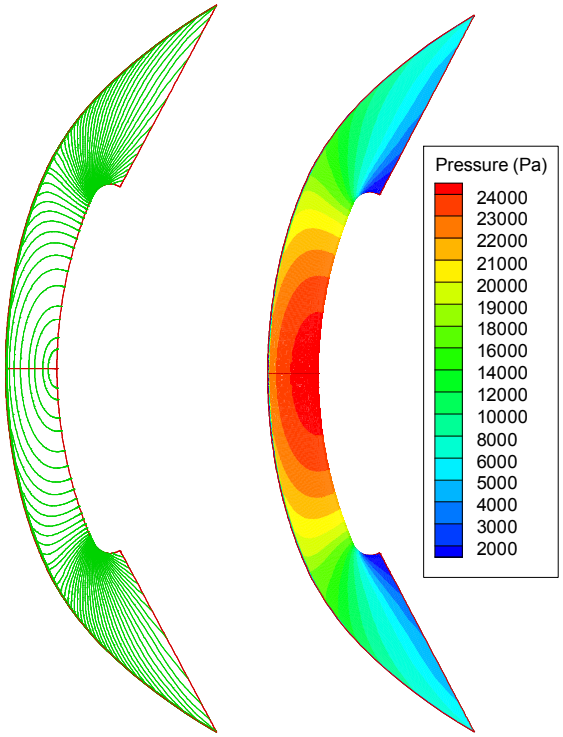

Figure 5.4. Pressure contour plot indicating a converged CFD solution.

nitrogen were used, therefore γ should be considered as a single epistemic uncertain variable. It should be also noted that for the range of velocities and free-stream conditions considered in the CFD study, no dissociated nitrogen exists in the flow, so the uncertainty in the recombination efficiency mainly affects the recombination of oxygen atoms on the surface.

Heat transfer to the surface of the vehicle is also strongly dependent on the total enthalpy of the flow, hence the free stream velocity. The variation in free stream velocity can be described through probabilistic measures due to its inherent nature. For the current study, the freestream velocity input to the CFD simulation is treated as an aleatoric uncertain variable with a uniform distribution with a mean of 2922 m/s (freestream condition given in Table 4.1). The upper and lower bounds for velocity were taken to be $\pm 3\%$ from the mean which corresponds to 2834.34 m/s and 3009.66 m/s respectively. For the freestream velocity uncertainty range, preliminary CFD results along with the model problem demonstrated the effects of velocity on the stagnation heat transfer to the vehicle to be fairly linear. Therefore, three collocation

points (V= 2834.34, 2922.0, and 3009.66 m/s) were sufficient to accurately describe and capture the change in heat flux as a function of freestream velocity at a given γ value.

Bose et al. [3] showed that the largest variation in heat flux to a Mars entry vehicle due to wall catalytic parameters occurred in moderately catalytic wall regime where γ_{cat} in their reactions ranged between 10^{-3} and 10^{-1}. Preliminary results of the current study have also demonstrated the same type of trend for air. For the velocity range and the wall temperature considered in this study, the change in surface heat transfer was found to be negligible for γ values above 0.5. Based upon these results, the interval bounds for γ was taken to be 0.001 and 0.5. Variation in heat transfer to the surface was extremely sensitive to changes in γ in the lower end of the interval. Therefore, the collocation points were selected to optimally capture the trend and accurately fit a response to the exponential growth curve. Furthermore, the actual uncertainty analysis was performed by taking $log_{10}(\gamma)$ as an epistemic uncertain variable instead of γ. This approach improved the quality and the convergence of stochastic response surface obtained with the NIPC approach. A total number of ten recombination efficiency values were selected to capture the change in heat flux due to variations in $log_{10}(\gamma)$ within the moderately catalytic regime at a given velocity. These 10 values were held consistent at all three velocities which gave a total number of 30 collocation points. This was sufficient for a 5^{th} order polynomial chaos expansion for two uncertain variables with a over-sampling ratio of 1.4. The deterministic CFD solutions were obtained at these collocation points and the Point-Collocation NIPC method was utilized to calculate the stochastic expansion for the surface heat transfer.

5.4. UNCERTAINTY QUANTIFICATION IN AEROHEATING

5.4.1. Results with Purely Aleatoric Uncertainty Assumption. Before the mixed uncertainty analysis, uncertainty quantification was conducted with the assumption of purely aleatoric input uncertainty. The results presented in this

section is later compared to the mixed uncertainty quantification results to show the difference between two uncertainty quantification approaches. For purely aleatoric uncertainty modeling, besides freestream velocity, the $[log_{10}(\gamma)]$ was also assumed to have a uniform distribution (changing between -3 and -0.301). The Point Collocation NIPC was utilized to propagate the uncertainty in $log_{10}(\gamma)$ and freestream velocity through the CFD simulations using the collocation points described in the previous section. It is important to ensure that the polynomial order is sufficient to capture the non-linear effects of the uncertainty in the output variable of interest. Therefore, a convergence study was conducted in which the polynomial order was increased up to 5 and the stagnation point heat transfer was analyzed at each order. Figure 5.5 shows the CDF of stagnation point heat transfer for each polynomial order. There is no noticeable difference in CDFs beyond a polynomial order of 3. Therefore, it is clear that NIPC response surface was converged at the 5^{th} order.

Figure 5.6 displays the probability density function (PDF) for the stagnation point heat transfer using 5^{th} order NIPC. This distribution is fairly non-linear and

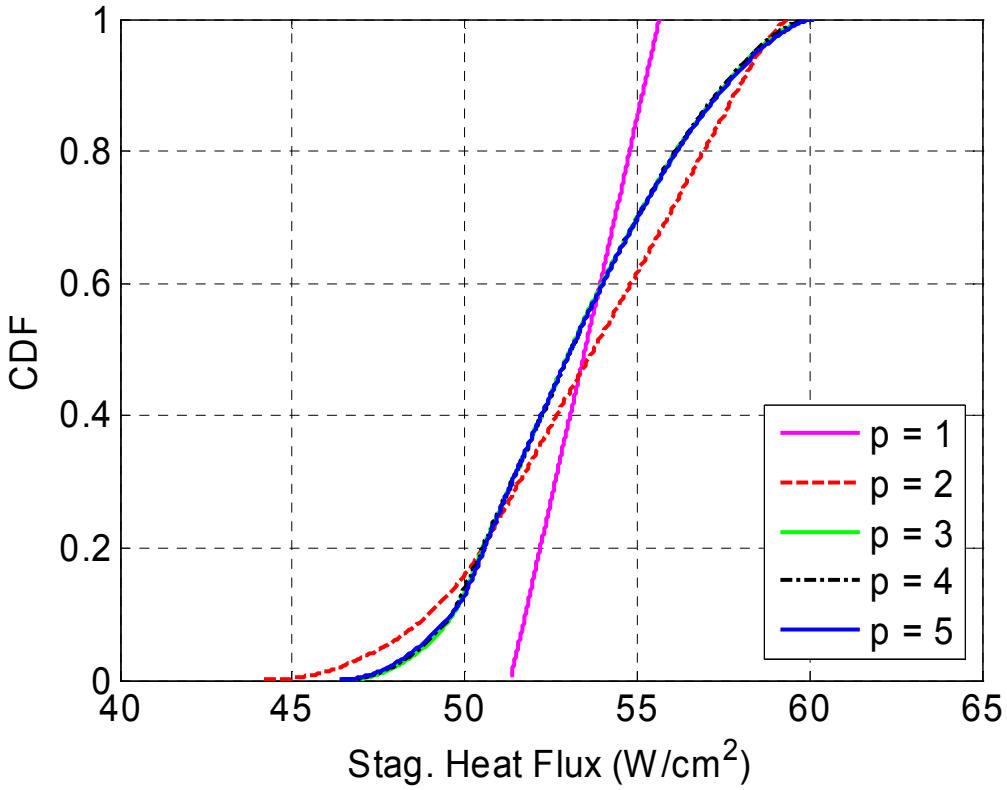

Figure 5.5. Convergence of NIPC response surface.

skewed which demonstrates the non-linear relationship between the uncertain variables and the stagnation point heat transfer, mostly due to γ. This can also be seen from the NIPC response surface for stagnation point heat transfer shown in Figure 5.7. Notice that the effects on the heat transfer due to velocity is fairly linear, whereas the effect due to $\log_{10}(\gamma)$ is quite non-linear. Furthermore, other statistical information can be calculated using NIPC, such as the mean and the standard deviation, since this analysis is made with the assumption of purely aleatory uncertainty. The mean stagnation point heat transfer was found to be 53.45 W/cm^2 and the standard deviation was calculated to be 2.99 W/cm^2 (e.g., a coefficient of variation of 5.6%). The 95% confidence interval (CI) for stagnation heat transfer was calculated as [46.05, 60.02] W/cm^2. Figure 5.8 displays the mean heat transfer along the surface of the vehicle along with the 95% confidence intervals (C.I.) at selected points. The fairly large standard deviation and CI values are indicative of the large amount of uncertainty in the heat flux to the surface of the vehicle.

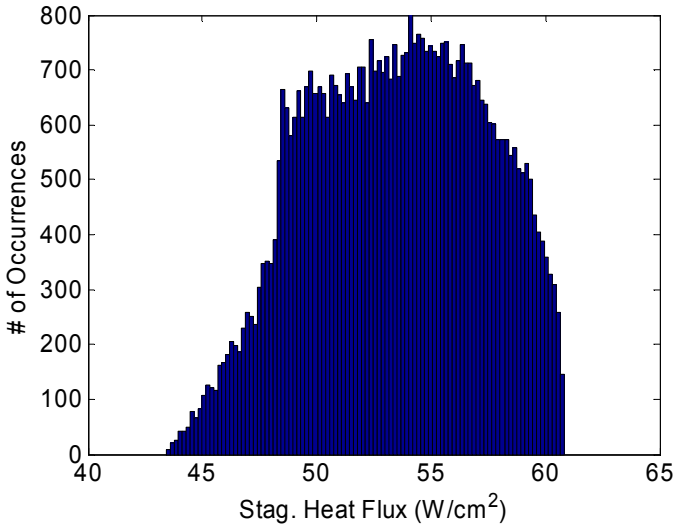

Figure 5.6. PDF curve for 5^{th} order NIPC.

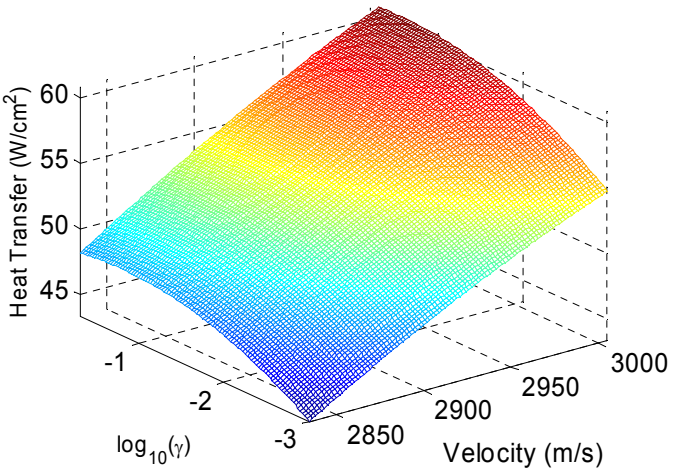

Figure 5.7. NIPC response surface (p = 5).

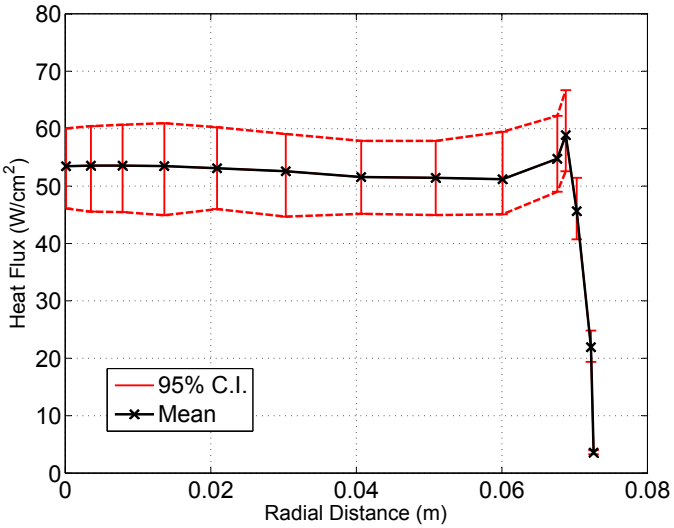

Figure 5.8. Mean and 95% C.I. for surface heat flux distribution (purely aleatoric uncertainty assumption).

5.4.2. Results with Mixed (Aleatory-Epistemic) Uncertainty Assumption. For the mixed uncertainty propagation, the same stochastic response surface used for purely aleatory uncertainty quantification (5^{th} degree polynomial chaos expansion for heat transfer) was utilized in Second-Order Probability approach. The outer loop utilized 20,000 values for the epistemic uncertain variable ($log_{10}(\gamma)$) sampled from its specified interval. In the inner loop, for each value of the epistemic uncertain variable, the stochastic response surface was evaluated with a total number of 10,000 randomly produced samples based on the standard probability distribution

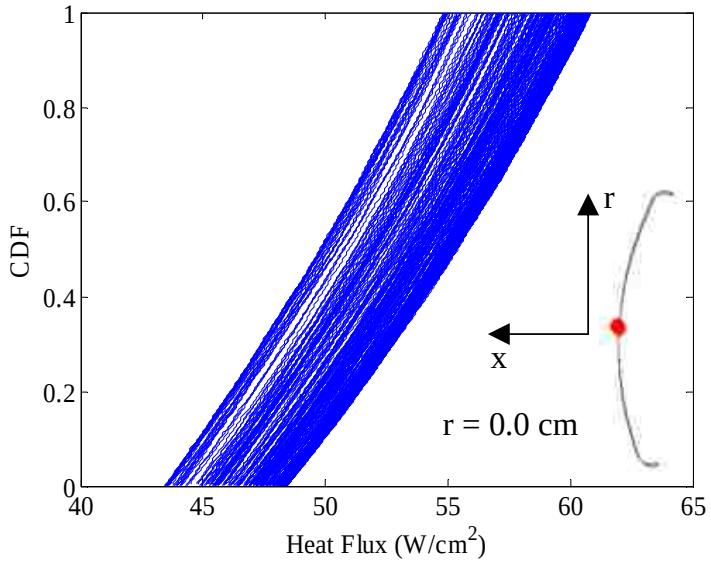

Figure 5.9. Second-Order Probability results for surface heat transfer at the stagnation point.

of the aleatoric input uncertainty (standard uniform distribution in this problem due to the uniform distribution assumption made for the velocity). This procedure was used to produce 20,000 CDFs, which were then evaluated to find the upper and the lower bounds of the interval for heat transfer at each probability level.

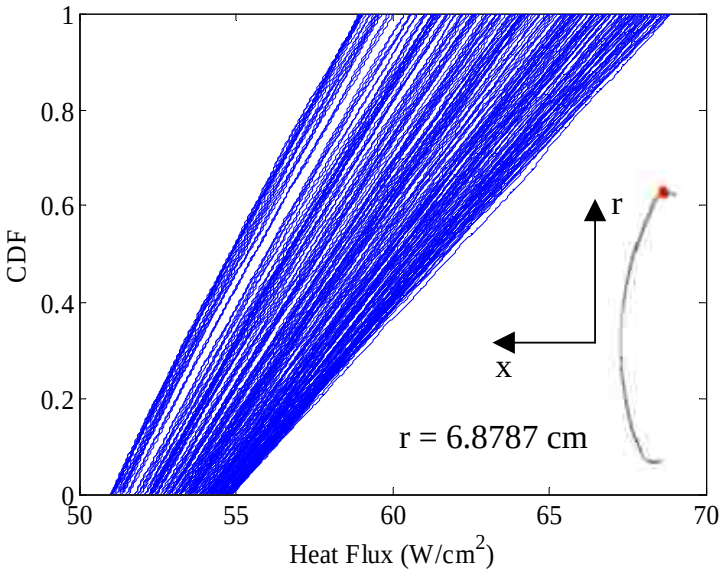

Figure 5.10. Second-Order Probability results for surface heat transfer at the shoulder region.

Table 5.1. Surface heat transfer (W/cm^2) for the stagnation point and the shoulder region at different probability levels for the CFD problem.

Probability Level	Stagnation Point Mixed Uncertainty	Stagnation Point Aleatory Uncertainty	Shoulder Mixed Uncertainty	Shoulder Aleatory Uncertainty
P = 0.0	[43.37, 48.43]	43.41	[50.93, 54.90]	50.96
P = 0.2	[45.90, 51.49]	49.76	[52.32, 57.72]	55.34
P = 0.4	[48.46, 54.24]	52.36	[53.88, 60.56]	57.44
P = 0.6	[50.74, 56.70]	54.74	[55.45, 63.42]	59.63
P = 0.8	[52.80, 58.89]	57.16	[57.60, 66.20]	62.39
P = 1.0	[54.75, 60.82]	60.81	[58.81, 68.92]	68.84

The mixed uncertainty results for the heat transfer at the stagnation point and shoulder regions are plotted in Figures 5.9 and 5.10. Note that at a particular probability level, the variation in the the heat transfer is due to the uncertainty in the recombination efficiency ($log_{10}(\gamma)$, epistemic uncertainty), which is represented by the interval bounded by the maximum and the minimum heat transfer values obtained from the CDF samples at the same probability level. In the stagnation region, the width of the interval at each probability level is fairly constant. In contrast, the interval bounds tend to increase at higher probability levels in the shoulder region as can be also seen quantitatively in Table 5.1. The pure aleatory results from the CFD simulations are also listed in Table 5.1 for comparison purposes. As expected, the stagnation heat flux from the purely aleatory uncertainty quantification lies within the bounds of the Second-Order Probability results. At the probability levels 0% and 100%, the purely aleatory heat transfer values are located at the boundaries of the corresponding intervals (lower and upper respectively).

The interval bounds for the heat transfer were plotted at selected points across the surface of the reentry vehicle at the 2.5%, 50%, and 97.5% probability levels. The resulting plots are shown in Figures 5.11, 5.12, and 5.13. Furthermore, the pure aleatory NIPC results are also shown in the figures at the corresponding probability levels. Notice that the pure aleatory is once again just a single value at each probability value at each point along the surface. In contrast, the mixed uncertainty results

are given as an intervals along the surface of the reentry vehicle. At probability level 2.5%, the pure aleatory values stay almost in the center of the mixed uncertainty intervals at most of the surface points except the shoulder region. Furthermore, the interval size is fairly constant along the surface of the vehicle. At probability level 50%, the pure aleatory values skew towards the upper bound of the mixed uncertainty interval. Also, the interval size slightly increases moving from the stagnation to the shoulder region along the surface. Furthermore, the size of the interval is larger for 50% when compared to the 2.5% probability level. At probability level 97.5%, the pure aleatory values lie almost at the upper limits of the aleatory-epistemic interval. There is a significant increase in the size of the interval near the shoulder region, consistent with the observation made from Figures 5.9 and 5.10.

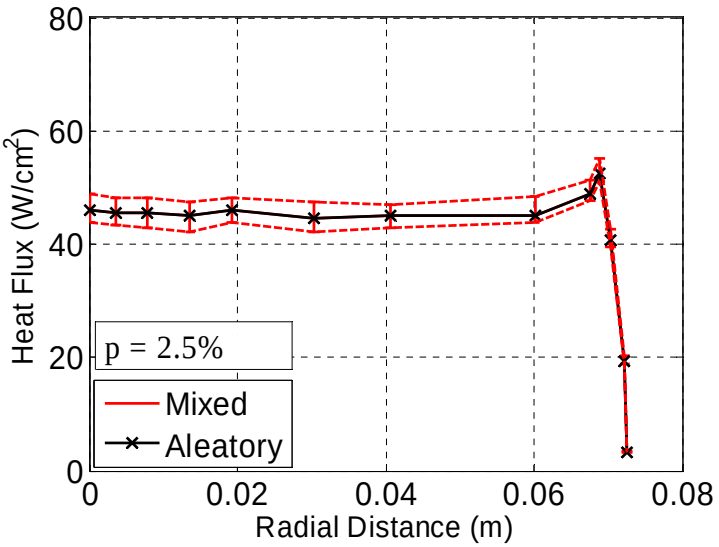

Figure 5.11. Comparison of pure aleatory and mixed aleatory-epistemic uncertainty results for surface heat transfer (Probability level 2.5%).

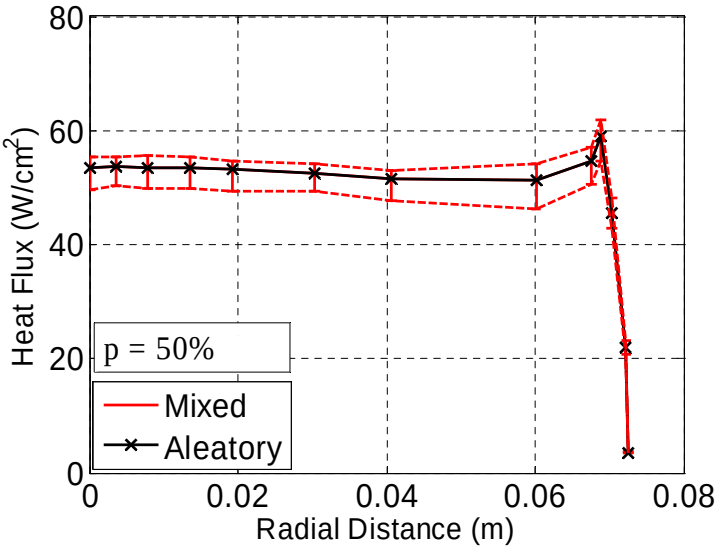

Figure 5.12. Comparison of pure aleatory and mixed aleatory-epistemic uncertainty results for surface heat transfer (Probability level 50%).

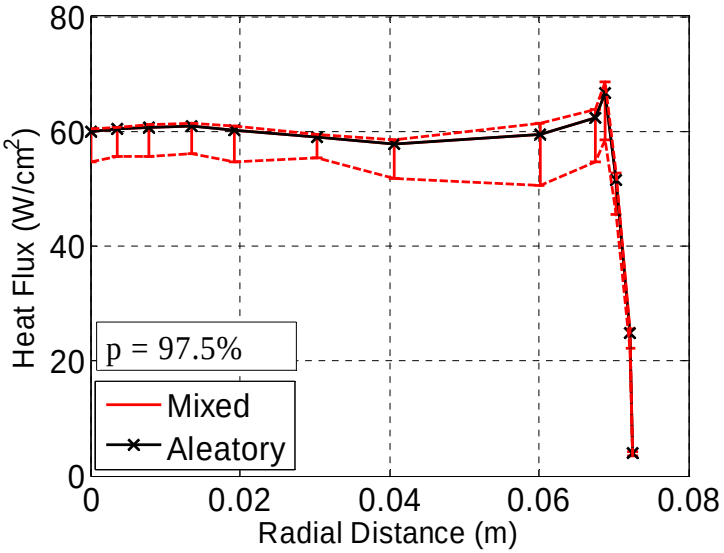

Figure 5.13. Comparison of pure aleatory and mixed aleatory-epistemic uncertainty results for surface heat transfer (Probability level 97.5%).

5.5. SENSITIVITY ANALYSIS

The global linear SA was also used for the CFD problem to provide the relative importance of each of the two uncertain variables, freestream velocity and $log_{10}(\gamma)$, on the overall uncertainty in the stagnation point heat transfer. To be consistent with the uncertainty analysis described above, the same 5^{th} order NIPC response surface was used for Monte Carlo (MC) simulation with 20,000 samples to obtain SA results. Scatter plots are shown in Figures 5.14 and 5.15 indicating the stagnation point heat transfer for various combinations of velocity and $log_{10}(\gamma)$. Figure 5.14 shows the stagnation point heat transfer as a function of freestream velocity and Figure 5.15 displays the stagnation heat transfer as a function of $log_{10}(\gamma)$. For this problem also, the freestream velocity has a higher relative importance on the overall stagnation point heat transfer. The correlation coefficient (CC) was calculated using linear regression [32] and is imposed on the plots in Figures 5.14 and 5.15. The CC

is approximately 0.9 for the velocity and approximately 0.4 for $log_{10}(\gamma)$, which again demonstrates that velocity has a stronger contribution to the overall uncertainty in the stagnation point heat transfer.

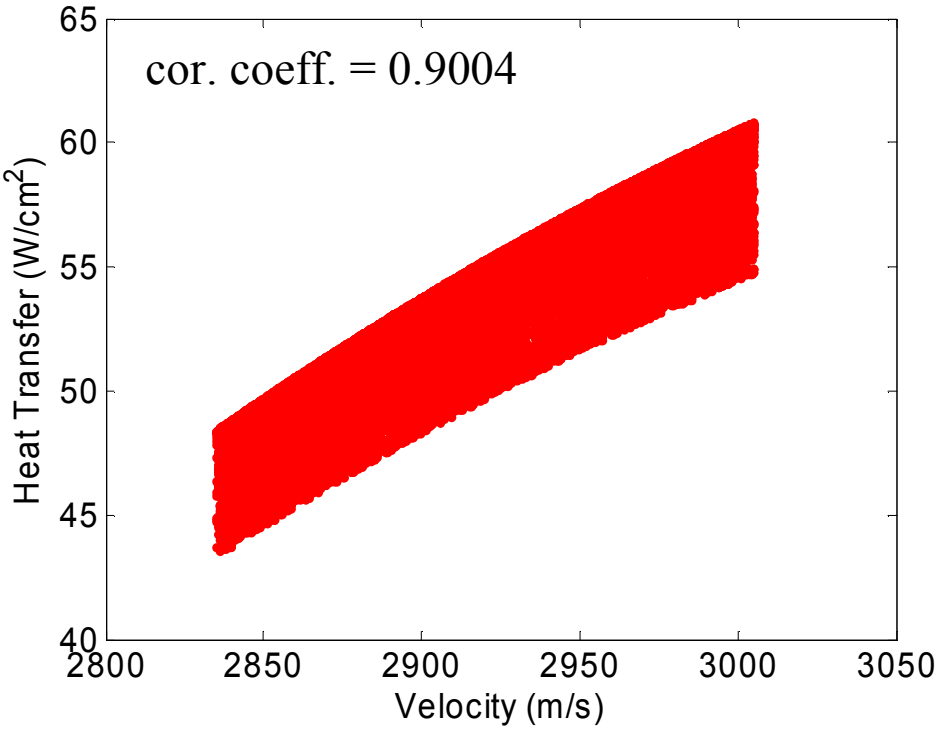

Figure 5.14. Correlation plots demonstrating the influence of velocity on the overall uncertainty in the stagnation heat flux.

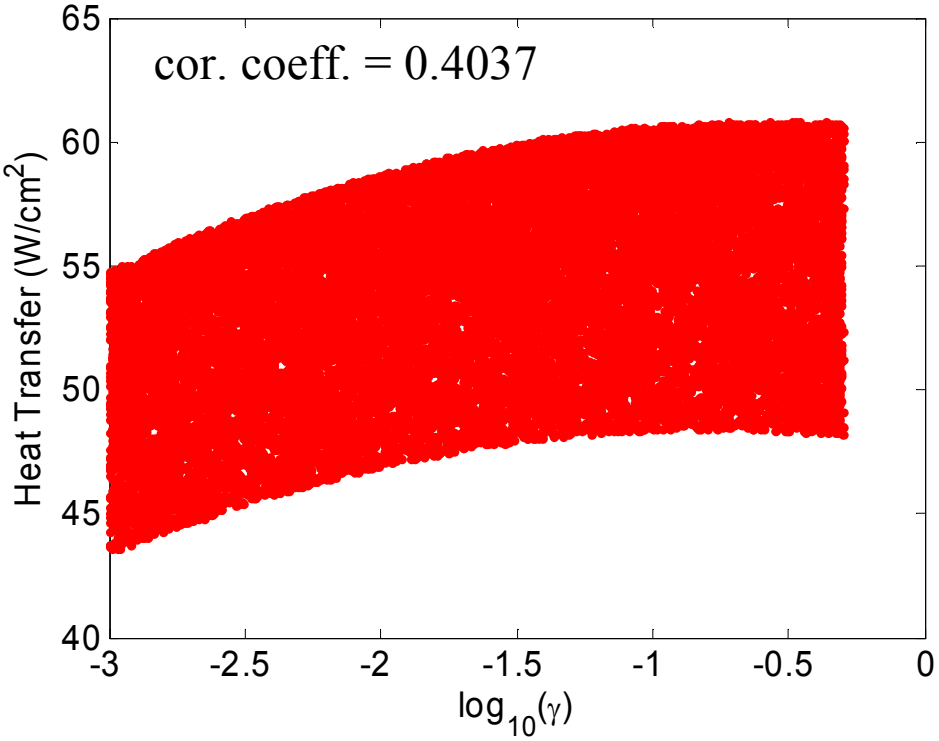

Figure 5.15. Correlation plots demonstrating the influence of $log_{10}(\gamma)$ on the overall uncertainty in the stagnation heat flux.

6. CONCLUSIONS AND FUTURE WORK

6.1. CONCLUSIONS

The primary focus of this study was to demonstrate an efficient approach for uncertainty quantification of surface heat flux to the spherical non-ablating heat-shield of a reentry vehicle due to epistemic and aleatory uncertainties that may exist in various parameters used in the numerical solution of hypersonic, viscous, laminar blunt-body flows with thermo-chemical non-equilibrium. In specific, the freestream velocity (V_∞) and the recombination efficiency (γ) of oxygen and nitrogen atoms used in the description of catalytic wall boundary condition were treated as uncertain variables. The freestream velocity was modeled as an inherent uncertain variable described with a uniform probability distribution, whereas the recombination efficiency was modeled as an epistemic uncertain variable represented with an interval. For the quantification of mixed (the aleatory-epistemic) uncertainty, Second-Order Probability Theory that utilized a stochastic response surface obtained with Point-Collocation Non-Intrusive Polynomial Chaos (NIPC) Method was used.

Before the implementation of the uncertainty quantification method to the stochastic high-fidelity CFD problem, the approach was applied to a stochastic model problem for the prediction of stagnation point heat transfer with Fay-Riddell relation, which considered velocity as an inherent uncertain variable and the boundary layer edge dynamic viscosity as an epistemic uncertain variable. For the model problem, the Second-Order Probability was implemented with two different approaches for the propagation of mixed uncertainty: (1) direct Monte Carlo sampling and (2) a 3^{rd} order stochastic response surface obtained with the Point-Collocation NIPC. The uncertainty results for the stagnation point heat transfer obtained with two approaches

matched well indicating the computational efficiency and the accuracy of the NIPC approach for mixed uncertainty propagation.

The uncertainty quantification in CFD simulations of the current study was performed for a particular test case and capsule geometry selected from the work of MacLean et al. [2], where the freestream velocity for the experiment was 2922 m/s. For the stochastic CFD problem, the mixed uncertainty quantification approach was utilized with a 5^{th} degree stochastic response surface obtained with the Point-Collocation NIPC, which required 30 deterministic simulations. The uncertainty in surface heat transfer was obtained in terms of intervals at different probability levels at various locations including the stagnation point and the shoulder region. The mixed uncertainty results were compared to the results obtained with a purely aleatory uncertainty analysis to show the difference between two uncertainty quantification approaches. A linear global sensitivity analysis indicated that the velocity has a stronger contribution to the overall uncertainty in the stagnation point heat transfer.

Overall, the results obtained in this study show the potential of the uncertainty quantification approach that utilizes Second-Order Probability and the Non-Intrusive Polynomial Chaos for efficient and effective propagation of mixed (aleatory and epistemic) uncertainties in high-fidelity hypersonic flow simulations including re-entry problems and the prediction of uncertainty in aerodynamic heating, which can be used for the design of reliable and optimized thermal protection systems.

6.2. FUTURE WORK

There are several tasks that remain as future work in the area of uncertainty quantification for hypersonic flow applications. For example, more relevant epistemic uncertainties could be introduced into the hypersonic reentry problem. If the flow is not laminar, then uncertainties in transition and turbulence modeling parameters can be investigated. Another aspect to be studied is the uncertainty in the collision integral curve fits used to model the transport quantities due to the fact that they can have a significant impact on the heat transfer to the vehicle's surface. Higher

freestream velocities, and thus higher stagnation enthalpies, will be used for future CFD runs to amplify the effects of uncertainty in the transport quantities as well as the recombination efficiency. Other types of aleatory uncertainties, such as geometric uncertainty, will also be investigated.

In future work, a slightly different technique for Second-Order Probability method with the NIPC response surface formulation will be investigated. In the current study, a large number of samples are taken for the inner and outer loops of Second-Order Probability and these sample points are evaluated using the stochastic response surface. To improve the computational efficiency of the proposed UQ approach further, one can use an optimization technique rather than basic sampling of the inner and outer loops. An optimization routine can be used to find the minimum and maximum of the output variable at certain probability levels. This process requires much fewer function evaluations when compared with the simple sampling techniques and can provide the same level of accuracy.

Other capabilities to be investigated in the future will include non-linear sensitivity analysis to rank the relative importance of each input uncertainty. Sobol indices [40, 41] will be calculated and used for global sensitivity analysis to determine higher-order correlation between input and output uncertainties as well as mixed contributions of the input variables. Another possibility for future work will be to investigate importance sampling in the selection of collocation points used within the non-intrusive polynomial chaos.

The proposed mixed aleatory and epistemic uncertainty quantification method can also be applied to other vehicle configurations due to its non-intrusive nature. For example, B. Bettis, S. Hosder, and T. Winter (M4 Engineering) are currently developing a generic uncertainty quantification framework under a NASA project. The methods discussed in this document are being added as capabilities into the generic UQ framework. The framework will be implemented to quantify uncertainties in the predictive capabilities of integrated spacecraft, such as a reusable launch vehicle.

Uncertainties are generally ubiquitous in the analysis and design of highly complex engineering systems. The uncertainties associated with hypersonic flows can have significant effects on the overall design process of hypersonic vehicles. Therefore, one of the main goals for future work will be to integrate uncertainty quantification to the design of hypersonic vehicles for robust and reliable hypersonic systems (thermal protection systems, propulsion, etc.) and vehicles.

APPENDIX A

Thermodynamic Curve-fits: MATLAB Source Code

```
% ==========================================================================
% This is a MATLAB equivalent to tgas3 which finds the temperature of
% an equilibrium gas for a given density and pressure.
%
% Reference: Srinivasan, S., Tannehill, J. C., and Weilmuenster, K. J.,
% "Simplified Curve Fits for the Thermodynamic Properties of
% Equilibrium Air, NASA Technical Report, August, 1987.
% ==========================================================================

function H = Enthalpy_fnct_pres_rho(P,rho)

% Calculate Y,X, and Z based on inputs of Pres and density
Y = log10(rho/1.292);
X = log10(P/101300);
Z = X - Y;

% Coefficients of curve fit will vary depending on the value of
% Y and Z
if (Y > -0.5) && (Z <= 0.30)
    c1 = 1.4;
    c2 = 0;
    c3 = 0;
    c4 = 0;
    c5 = 0;
    c6 = 0;
    c7 = 0;
    c8 = 0;
    c9 = 0;
    c10 = 0;
    c11 = 0;

elseif (Y > -0.5) && (Z > 0.30) && (Z <= 1.15)
    c1 = 1.42598;
    c2 = 0.000918;
    c3 = -0.092209;
    c4 = -0.002226;
    c5 = 0.019772;
    c6 = -0.036600;
    c7 = -0.077469;
    c8 = 0.043878;
    c9 = -15;
    c10 = -1.0;
    c11 = -1.040;

elseif (Y > -0.5) && (Z > 1.15) && (Z <= 1.60)
    c1 = 1.64689;
    c2 = -0.062155;
    c3 = -0.334994;
    c4 = 0.063612;
    c5 = -0.038332;
    c6 = -0.014468;
    c7 = 0.073421;
    c8 = -0.002442;
    c9 = -15;
    c10 = -1.0;
    c11 = -1.360;

elseif (Y > -0.5) && (Z > 1.60)
```

```
    c1 = 1.48558;
    c2 = -0.453562;
    c3 = -0.152096;
    c4 = 0.303350;
    c5 = -0.459282;
    c6 = 0.448395;
    c7 = 0.220546;
    c8 = -0.292293;
    c9 = -10.0;
    c10 = -1.0;
    c11 = -1.600;

elseif (Y >-4.50) && (Y <= 0.5) && (Z <= 0.30)
    c1 = 1.4000;
    c2 = 0;
    c3 = 0;
    c4 = 0;
    c5 = 0;
    c6 = 0;
    c7 = 0;
    c8 = 0;
    c9 = 0;
    c10 = 0;
    c11 = 0;

elseif (Y >-4.50) && (Y <= 0.5) && (Z > 0.30) && (Z <= 0.98)
    c1 = 1.42176;
    c2 = -0.000366;
    c3 = -0.083614;
    c4 = 0.000675;
    c5 = 0.005272;
    c6 = -0.115853;
    c7 = -0.007363;
    c8 = 0.146179;
    c9 = -20.0;
    c10 = -1.0;
    c11 = -0.860;

elseif (Y >-4.50) && (Y <= 0.5) && (Z > 0.98) && (Z <= 1.38)
    c1 = 1.74436;
    c2 = -0.035354;
    c3 = -0.415045;
    c4 = 0.061921;
    c5 = 0.018536;
    c6 = 0.043582;
    c7 = 0.044353;
    c8 = -0.049750;
    c9 = -20.0;
    c10 = -1.04;
    c11 = -1.336;

 elseif (Y >-4.50) && (Y <= 0.5) && (Z > 1.38) && (Z <= 2.04)
    c1 = 1.49674;
    c2 = -0.021583;
    c3 = -0.197008;
    c4 = 0.030886;
    c5 = -0.157738;
    c6 = -0.009158;
```

```
    c7 = 0.123213;
    c8 = -0.006553;
    c9 = -10.0;
    c10 = -1.05;
    c11 = -1.895;

elseif (Y >-4.50) && (Y <= 0.5) && (Z > 2.04)
    c1 = 1.10421;
    c2 = -0.033664;
    c3 = 0.031768;
    c4 = 0.024335;
    c5 = -0.178802;
    c6 = -0.017456;
    c7 = 0.080373;
    c8 = 0.002511;
    c9 = -15.0;
    c10 = -1.08;
    c11 = -2.650;

elseif (Y >= -7.0) && (Y <= -4.5) && (Z <= 0.398)
    c1 = 1.400;
    c2 = 0;
    c3 = 0;
    c4 = 0;
    c5 = 0;
    c6 = 0;
    c7 = 0;
    c8 = 0;
    c9 = 0;
    c10 = 0;
    c11 = 0;

elseif (Y >= -7.0) && (Y <= -4.5) && (Z > 0.398) && (Z <= 0.87)
    c1 = 1.47003;
    c2 = 0.007939;
    c3 = -0.244205;
    c4 = -0.025607;
    c5 = 0.872248;
    c6 = 0.049452;
    c7 = -0.764158;
    c8 = 0.000147;
    c9 = -20.0;
    c10 = -1.0;
    c11 = -0.742;

elseif (Y >= -7.0) && (Y <= -4.5) && (Z > 0.87) && (Z <= 1.27)
    c1 = 3.18652;
    c2 = 0.137930;
    c3 = -1.89529;
    c4 = -0.103490;
    c5 = -2.14572;
    c6 = -0.272717;
    c7 = 2.06586;
    c8 = 0.223046;
    c9 = -15.0;
    c10 = -1.0;
    c11 = -1.041;
```

```
elseif (Y >= -7.0) && (Y <= -4.5) && (Z > 1.27) && (Z <= 1.863)
    c1 = 1.63963;
    c2 = -0.001004;
    c3 = -0.303549;
    c4 = 0.016464;
    c5 = -0.852169;
    c6 = -0.101237;
    c7 = 0.503123;
    c8 = 0.043580;
    c9 = -10.0;
    c10 = -1.0;
    c11 = -1.544;

elseif (Y >= -7.0) && (Y <= -4.5) && (Z > 1.863)
    c1 = 1.55889;
    c2 = 0.055932;
    c3 = -0.211764;
    c4 = -0.023548;
    c5 = -0.549041;
    c6 = -0.101758;
    c7 = 0.276732;
    c8 = 0.046031;
    c9 = -15.0;
    c10 = -1.0;
    c11 = -2.250;

else
    H = 'inputs not within acceptable range'

end

% Equation for calculating gamma_tilda
gamma_tilda = c1 + c2*Y + c3*Z + c4*Y*Z + (c5 + c6*Y + c7*Z + c8*Y*Z)/(1 ...
    + exp(c9*(X + c10*Y + c11)));

% Calculate the enthalpy
H = (P/rho)*(gamma_tilda/(gamma_tilda-1));
```

```
% ==========================================================================
% This is a MATLAB equivalent to tgas3 which finds the temperature of
% an equilibrium gas for a given density and pressure.
%
% Reference: Srinivasan, S., Tannehill, J. C., and Weilmuenster, K. J.,
% "Simplified Curve Fits for the Thermodynamic Properties of
% Equilibrium Air, NASA Technical Report, August, 1987.
% ==========================================================================

function T = Temp_fnct_rho_pres(P,rho)

check = 0;

% Calculate Y,X, and Z based on inputs of Pres and density
Y = log10(rho/1.225);
X = log10(P/101325);
Z = X - Y;

% Coefficients of curve fit will vary depending on the value of
% Y and Z
if (Y > -0.5) && (Z > 0.48) && (Z <= 0.90)
    d1 = 0.27407;
    d2 = 0;
    d3 = 1.00082;
    d4 = 0;
    d5 = 0;
    d6 = 0;
    d7 = 0;
    d8 = 0;
    d9 = 0;
    d10 = 0;
    d11 = 0;
    d12 = 0;

elseif (Y > -0.5) && (Z > 0.90)
    d1 = 0.235869;
    d2 = -0.043304;
    d3 = 1.17619;
    d4 = 0.046498;
    d5 = -0.143721;
    d6 = -1.37670;
    d7 = 0.160465;
    d8 = 1.08988;
    d9 = -0.083489;
    d10 = -0.217748;
    d11 = -10.0;
    d12 = -1.78;

elseif (Y > -4.5) && (Y <= -0.5) && (Z > 0.48) && (Z <= 0.9165)
    d1 = 0.281611;
    d2 = 0.001267;
    d3 = 0.990406;
    d4 = 0;
    d5 = 0;
    d6 = 0;
    d7 = 0;
    d8 = 0;
    d9 = 0;
```

```
    d10 = 0;
    d11 = 0;
    d12 = 0;

elseif (Y > -4.5) && (Y <= -0.5) && (Z > 0.9165) && (Z <= 1.478)
    d1 = 0.457643;
    d2 = -0.034272;
    d3 = 0.819119;
    d4 = 0.046471;
    d5 = 0;
    d6 = -0.073233;
    d7 = -0.169816;
    d8 = 0.043264;
    d9 = 0.111854;
    d10 = 0;
    d11 = -15.0;
    d12 = -1.28;

elseif (Y > -4.5) && (Y <= -0.5) && (Z > 1.478) && (Z <= 2.176)
    d1 = 1.04172;
    d2 = 0.041961;
    d3 = 0.412752;
    d4 = -0.009329;
    d5 = 0;
    d6 = -0.434074;
    d7 = -0.196914;
    d8 = 0.264883;
    d9 = 0.100599;
    d10 = 0;
    d11 = -15.0;
    d12 = -1.778;

elseif (Y > -4.5) && (Y <= -0.5) && (Z > 2.176)
    d1 = 0.418298;
    d2 = -0.252100;
    d3 = 0.784048;
    d4 = 0.144576;
    d5 = 0;
    d6 = -2.00015;
    d7 = -0.639022;
    d8 = 0.716053;
    d9 = 0.206457;
    d10 = 0;
    d11 = -10.0;
    d12 = -2.40;

elseif (Y >= -7) && (Y <= -4.5) && (Z > 0.30) && (Z <= 1.07)
    d1 = 2.72964;
    d2 = 0.003725;
    d3 = 0.938851;
    d4 = -0.011920;
    d5 = 0;
    d6 = 0.682406;
    d7 = 0.089153;
    d8 = -0.646541;
    d9 = -0.070769;
    d10 = 0;
    d11 = -20.0;
```

```
    d12 = -0.82;

elseif (Y >= -7) && (Y <= -4.5) && (Z > 0.30) && (Z <= 1.07)
    d1 = 2.72964;
    d2 = 0.003725;
    d3 = 0.938851;
    d4 = -0.011920;
    d5 = 0;
    d6 = 0.682406;
    d7 = 0.089153;
    d8 = -0.646541;
    d9 = -0.070769;
    d10 = 0;
    d11 = -20.0;
    d12 = -0.82;

elseif (Y >= -7) && (Y <= -4.5) && (Z > 1.07) && (Z <= 1.57)
    d1 = 2.50246;
    d2 = -0.042827;
    d3 = 1.12924;
    d4 = 0.041517;
    d5 = 0;
    d6 = 1.72067;
    d7 = 0.268008;
    d8 = -1.25038;
    d9 = -0.179711;
    d10 = 0;
    d11 = -20.0;
    d12 = -1.33;
elseif (Y >= -7) && (Y <= -4.5) && (Z > 1.57) && (Z <= 2.24)
    d1 = 2.44531;
    d2 = -0.047722;
    d3 = 1.00488;
    d4 = 0.034349;
    d5 = 0;
    d6 = 1.95893;
    d7 = 0.316244;
    d8 = -1.01200;
    d9 = -0.151561;
    d10 = 0;
    d11 = -20.0;
    d12 = -1.88;

elseif (Y >= -7) && (Y <= -4.5) && (Z > 2.24)
    d1 = 2.50342;
    d2 = 0.026825;
    d3 = 0.838860;
    d4 = -0.009819;
    d5 = 0;
    d6 = 3.58284;
    d7 = 0.533853;
    d8 = -1.36147;
    d9 = -0.195436;
    d10 = 0;
    d11 = -20.0;
    d12 = -2.47;

elseif (Z < 0.48) && (Y > -0.5)
```

```
    check = 1;
elseif (Z < 0.3)
    check = 1;

else
    T = 'inputs not within acceptable range'

end

if (check == 0)
    % Equation for calculating Temp (To is standard sea level condition)
    To = 273.2;     %Kelvin
    RHS = d1 + d2*Y + d3*Z +d4*Y*Z + d5*Z^2 + (d6 + d7*Y + d8*Z + d9*Y*Z...
        + d10*Z^2)/(1 + exp(d11*(Z + d12)));

    T = (10^RHS)*To;
    T = T/1.8;          % Temperature

else
    T = P/(rho*287);    % Temperature
end
```

APPENDIX B

Statistical Thermodynamics

One of the overarching goals of statistical thermodynamics is to relate the microstate (molecular level) of a fluid to the macrostate (measurable level). In other words, the goal is to relate the molecular movement of a fluid to the measurable thermodynamic quantities such as temperature and pressure. A microstate is defined as the state of a system inspected from the quantum, or molecular, level. Microstates are defined by the number of particles (N), characteristic energies (ϵ_j), and the number of quantum energy states (C_j) . Several assumptions must be made in order to accomplish the goal of relating the mass fractions for air as a function of the macrostate of the fluid system (temperature, pressure, etc.). The main assumption of statistical mechanics is that all possible microstates of a system (N, ϵ_j, and C_j) are equally probable. This is a valid assumption due to the fact that a system's microstate can constantly change due to intermolecular collisions and there is no reason for nature to prefer one microstate over another. Furthermore, the Boltzman limit states that the number of particles is much smaller than the number of energy states ($C_j \gg N_j$). This limit is indeed true in mostly all physical systems. Using the Boltzman limit, the specific macrostate which yields the most possible number of microstates (N^*) can be written as a function of temperature, number of particles, and the various quantum energy states and this is shown in Equation (B.1). Note that k is the Boltzman constant.

$$N_j^* = N\frac{C_j e^{-\epsilon_j/kT}}{\sum_j C_j e^{-\epsilon_j/kT}} \tag{B.1}$$

The denominator of Equation (B.1) is called the molecular partition function and it holds special significance in statistical mechanics. The partition function is defined as,

$$Q \equiv \sum_j C_j e^{-\epsilon_j/kT} \tag{B.2}$$

but it is generally more convenient to express it in terms of degeneracy (g_i) rather than energy groups. Degeneracy is defined as the number of all energy states having

identical values of energy ϵ_j. So the partition function can be rewritten as,

$$Q = \sum_i g_i e^{-\epsilon_i/kT} \tag{B.3}$$

Note that the change of subscripts from j to i in Equations (B.2) and (B.3) merely indicates the change from examining energy states (j) to energy levels (i). The partition function is the key link in relating the molecular state (microstate) of a physical system to the thermodynamic state properties that are generally of interest in fluid dynamic problems such as temperature, pressure, entropy, etc. Therefore, it is crucial to have a procedure for calculating the partition function.

The internal structure of a particle (atom or molecule) must be analyzed to calculate the partition function. More specifically, all of the various contributions from various energy modes, which sum to be the total energy of the particle, must be quantified. For this study, the possible energy modes for molecules are translational, vibrational, rotational, and electronic energy. Atoms will have translational and electronic energy modes, but they will obviously not have the rotational and vibrational energy modes. For analysis sake, assume the following discussion pertains to a molecule which has the four energy modes mentioned here. The total particle energy will be the summation of each contributing energy mode, which can be seen in Equation (B.4).

$$\epsilon = \epsilon_{trans} + \epsilon_{rot} + \epsilon_{vib} + \epsilon_{el} \tag{B.4}$$

Now recall the formula for the partition function from Equation (B.3). Also recall that the entire set of possible energy states is translational, rotational, vibrational, and electronic energy. Therefore, the summation in Equation (B.3) can be broken into four separate summations, mainly translational, rotational, vibrational,

and electronic energy.

$$Q = \sum_i g_i e^{-\epsilon_i/kT} = g_i \left(\sum_{trans} e^{-\epsilon_i/kT} \right) \left(\sum_{rot} e^{-\epsilon_i/kT} \right) \left(\sum_{vib} e^{-\epsilon_i/kT} \right) \left(\sum_{el} e^{-\epsilon_i/kT} \right) \tag{B.5}$$

Using the relation of the partition function in Equation (B.3), this can be rewritten in terms of partition functions alone.

$$Q = Q_{trans} Q_{rot} Q_{vib} Q_{el} \tag{B.6}$$

Recall that Equation (B.6) represents the overall partition function of a molecule in terms of each energy mode. For an atomic particle, only the translational and electronic energy modes will be present. Therefore, the overall partition function of an atomic particle is written as:

$$Q = Q_{trans} Q_{el} \tag{B.7}$$

Using statistical thermodynamics, the partition functions can now be written in a useful manner. The entire derivation for the partition functions can be seen in the textbook by Vincenti and Kruger [31] but due to space constraints and objectivity only the final form of the partition functions will be given. The partition function for the translation energy mode is (Vincenti and Kruger [31]),

$$Q_{trans} = \left(\frac{2\pi m k T}{h^2} \right) \tag{B.8}$$

where m is the molecular mass, k is the Boltzman constant, T is the translational temperature, and h is Planck's constant ($6.63 \times 10^{-34} \frac{kg \cdot m^2}{s}$). Assuming a rigid rotor model for diatomic molecules, the partition function for rotational energy mode can be shown to be the following (Vincenti and Kruger [31]),

$$Q_{rot} = \frac{T}{\Theta_r} \tag{B.9}$$

where Θ_r is the characteristic temperature of rotation. Values of Θ_r vary for different molecular species, and typical values can be found in Vincenti and Kruger [31]. Next, the partition function for the vibrational energy mode can be derived utilizing a harmonic oscillator assumption for the molecule. The final form of the partition function is (Vincenti and Kruger [31]),

$$Q_{vib} = \frac{1}{1 - e^{-\Theta_v/T}} \tag{B.10}$$

where Θ_v is the characteristic temperature of vibration. Once again, Θ_v can vary depending on the molecular species and typical values for the applicable species can be found in Vincenti and Kruger [31]. Lastly, the partition function for the electronic energy mode can be reduced to (Vincenti and Kruger [31]),

$$Q_{el} = g_0 + g_1 e^{-\Theta_1/T} \tag{B.11}$$

where g_0 and g_1 is the degeneracy at the ground state and first energy level, respectively, and Θ_1 is the characteristic temperature for electronic excitation. These values are generally known from spectroscopy experiments and typical values can be obtained in Vincenti and Kruger [31].

Now that the partition functions for each energy mode is explicitly written in terms of known quantities, the next step is to apply the law of mass action to find the equilibrium composition of air as a function of temperature and pressure. Vincenti and Kruger [31] describe the process for deriving the law of mass action for an ideal dissociating gas. The final form of the equation is written below.

$$\frac{\alpha^{*2}}{1 - \alpha^*} = \frac{\rho_d}{\rho} e^{-\Theta_d/T} \tag{B.12}$$

In Equation (B.12), ρ_d is the characteristic density for dissociation and Θ_d is the dissociation temperature. Values for ρ_d and Θ_d vary for O_2 and N_2 and typical values can be found in Vincenti and Kruger [31]. Furthermore, α^* is known as the degree of

dissociation and is defined as the following (Vincenti and Kruger [31]).

$$\alpha^* = \frac{mass\ of\ dissociated\ i-atom}{total\ mass\ of\ gas} \tag{B.13}$$

The characteristic density for dissociation can be written as (Vincenti and Kruger [31]),

$$\rho_d = \frac{m\left(Q^a\right)^2}{2VQ^{aa}} = const. \tag{B.14}$$

which can be shown to be a constant value for most conventional high temperature systems. The next step is to solve the quadratic equation in Equation (B.12) for α^*. This can be done using any root finding method, but for this study a built in function in MATLAB was used to solve for α^*.

The degree of dissociation of each species can now be calculated using the procedure described above. There is now enough information to calculate the equilibrium constants which will be directly used to calculate the partial pressures of each species of air present behind the normal shock. To find the equilibrium constant, rewrite Equation (B.12) as

$$\frac{\alpha^{*2}}{1-\alpha^*} = \frac{G\left(T\right)}{\rho} \tag{B.15}$$

where,

$$G(T) = \rho_d e^{-\Theta_d/T} \tag{B.16}$$

The details will not be shown here, but Vincenti and Kruger derived a relationship between $G(T)$ and the equilibrium constant $K(T)$. The final form is given in Equation (B.17).

$$\frac{2kT}{m_{i,a}} G(T) = K\left(T\right) \tag{B.17}$$

APPENDIX C

Fay-Riddell Model Problem: MATLAB Source Code

```
%==========================================================================
% Author: Ben Bettis
% Date: 1/21/2010
% Purpose: This program approximates the heat transfer to a reentry
% vehicle using the Fay Riddell equation. To do this, the properties
% behind an equilibrium normal shock must be calculated. Then, the
% equilibrium composition of air is found using statistical
% mechanics. Finally, these quantities are inserted into Fay Riddel
% equation to find the heat flux.
%==========================================================================
function q = Monte_Carlo_Heat_flux_reentry_vehicle(u1,k_visc)

format 'long'

%==========================================================================
% First step is to calculate the equilibrium properties across a
% normal shock wave given that the freestream conditions are known.
%==========================================================================

n = 1;

for q = 1:n
    Rn = 0.17526;
    % Thermochemical Equilibrium Analysis
    % Free stream flow conditions
    T1 = 522;        % Temperature
    % Mass fraction N_2
    c_N2 = 0.001168/(0.001168+0.0002719+0.0001041+0.00004596);
    % Mass fraction O_2
    c_O2 = 0.0002719/(0.001168+0.0002719+0.0001041+0.00004596);
    % Mass fraction NO
    c_NO = 0.0001041/(0.001168+0.0002719+0.0001041+0.00004596);
    % Mass fraction N
    c_N = 0/(0.001168+0.0002719+0.0001041+0.00004596);
    % Mass fraction O
    c_O = 0.00004596/(0.001168+0.0002719+0.0001041+0.00004596);

    % Calculate the gas constant of the mixture
    R_mix = ((296.939*c_N2)+(259.822*c_O2)+(277.143*c_NO)+...
        (593.8786*c_N)+(519.64375*c_O))/(c_N2+c_O2+c_NO+c_O+c_N);
    % Density of the mixture
    rho1 = 0.001168+0.0002719+0.0001041+0.00004596;
    % Pressure of the mixture
    P1 = rho1*R_mix*T1;
    % Enthalpy of the mixture
    H1=Enthalpy_fnct_pres_rho(P1,rho1);
    % Mach number
    Mach = u1/sqrt(1.4*287*T1);
    % Wall temperature (K)
    Twall = 300;

    % Use the root finding Secant Method to solve for the properties
    % behind the normal shock wave.

    %first guess for the density ratio
    epsilon(1,1) = 0.001;
    epsilon(2,1) = 0.1;
```

```
P(1,1)=P1+rho1*u1^2*(1-epsilon(1,1));
rho2(1,1)=rho1/epsilon(1,1);
h2(1,1) = H1 + (u1^2/2)*(1-epsilon(1,1)^2);

% Thermodynamic curve-fits (enthalpy as function of temp & rho)
h2_tilda(1,1) = Enthalpy_fnct_pres_rho(P(1,1),rho2(1,1));
dH(1,1) = h2_tilda(1,1) - h2(1,1);
P(2,1)=P1+rho1*u1^2*(1-epsilon(2,1));
rho2(2,1)=rho1/epsilon(2,1);
h2(2,1) = H1 + (u1^2/2)*(1-epsilon(2,1)^2);
h2_tilda(2,1) = Enthalpy_fnct_pres_rho(P(2,1),rho2(2,1));
dH(2,1) = h2_tilda(2,1) - h2(2,1);
epsilon(3,1) = epsilon(2,1) - dH(2,1)/((dH(2,1)-dH(1,1))/...
    (epsilon(2,1)-epsilon(1,1)));

% Proceed on with the Secant Method for 25 iterations or until the
% convergence criteria of 10^-6 is met
for n = 3:25
    P(n,1)=P1+rho1*u1^2*(1-epsilon(n,1));
    rho2(n,1)=rho1/epsilon(n,1);
    h2(n,1) = H1 + (u1^2/2)*(1-epsilon(n,1)^2);
    h2_tilda(n,1) = Enthalpy_fnct_pres_rho(P(n,1),rho2(n,1));
    dH(n,1) = h2_tilda(n,1) - h2(n,1);
    convergence = abs(dH(n,1)/h2(n,1));

    % Check the convergence criteria
    if (convergence < 10^-6) break
    end

    epsilon(n+1,1) = epsilon(n,1) - dH(n,1)/((dH(n,1)-dH(n-1,1))/...
        (epsilon(n,1)-epsilon(n-1,1)));
end

% Calculate properties behind the normal shock wave (results of the
% Secant Method)
H2 = h2_tilda(n,1);
% Thermodynamic curve-fits (temperature as function of temp & rho)
T2 = Temp_fnct_rho_pres(P(n,1),rho2(n,1));
P2 = P(n,1);
Rho2 = rho2(n,1);
U2 = epsilon(n,1)*u1;

%=========================================================
% Next step is to find the equilibrium composition of the air
% behind the normal shock wave based on the pressure and
% temperature values just found.
%=========================================================

% Calculate the mass of each species
m_N2 = 28/(6.023*10^26); m_N = 14/(6.023*10^26);...
    m_O = 16/(6.023*10^26); m_O2 = 32/(6.023*10^26);...
    m_NO = 30/(6.023*10^26);

k = 1.38*10^-23;      % Boltzman's constant
V = 1;                % Volume

% Characteritic temperature of vibration
thetav_N = 3390; thetav_O = 2270; thetav_NO = 2740;
```

```
% Characteritic temperature of rotation
thetar_N = 2.9; thetar_O = 2.1; thetar_NO = 2.5;
% Characteritic temperature of dissociation
thetad_N = 113000; thetad_O = 59500; thetad_NO = 75500;

h = 6.63*10^-34;    % Planck's Constant

% Redefine naming conventions for simplicity of programming
rho = Rho2;
T = T2;
temp = T2/thetad_N;

%=========================================================================

% Now calculate partition functions for each species
% Nitrogen
Qtr_N = (2*pi*m_N*k*T/(h^2))^1.5;          % Translational
Qtr_N2 = (2*pi*m_N2*k*T/(h^2))^1.5;        % Translational
Qrot_N = 0.5*T/thetar_N;                   % Rotational
Qv_N = (1-exp(-thetav_N/T))^-1;            % Vibrational
Qel_N = 4;                                 % Electronic
Qel_N2 = 1;                                % Electronic
Q_tot_atom_N = Qtr_N*Qel_N;
Q_tot_mol_N = Qtr_N2*Qrot_N*Qv_N*Qel_N2;

% Oxygen
Qtr_O = (2*pi*m_O*k*T/(h^2))^1.5;          % Translational
Qtr_O2 = (2*pi*m_O2*k*T/(h^2))^1.5;        % Translational
Qrot_O = 0.5*T/thetar_O;                   % Rotational
Qv_O = (1-exp(-thetav_O/T))^-1;            % Vibrational
Qel_O = 5+3*exp(-228/T)+exp(-326/T);       % Electronic
Qel_O2 = 5;                                % Electronic
Q_tot_atom_O = Qtr_O*Qel_O;
Q_tot_mol_O = Qtr_O2*Qrot_O*Qv_O*Qel_O2;

% Nitric Oxide
Qtr_NO = (2*pi*m_NO*k*T/(h^2))^1.5;        % Translational
Qrot_NO = 0.5*T/thetar_NO;                 % Translational
Qv_NO = (1-exp(-thetav_NO/T))^-1;          % Rotational
Qel_NO = 2+2*exp(-174/T);                  % Vibrational
Q_tot_atom_NO = Q_tot_atom_O*Q_tot_atom_N; % Electronic
Q_tot_mol_NO = Qtr_NO*Qrot_NO*Qv_NO*Qel_NO; % Electronic

%=========================================================================

% Degree of dissociation calculations -- Nitrogen
LHS_N = (m_N/(2*rho))*(Q_tot_atom_N^2/Q_tot_mol_N)*exp(-thetad_N/T);
aa = [1 LHS_N -LHS_N];
root_finder = roots(aa);
dod_N = root_finder(2,1);
GT_N = LHS_N*rho;

% Degree of dissociation calculations -- Oxygen
LHS_O = (m_O/(2*rho))*(Q_tot_atom_O^2/Q_tot_mol_O)*exp(-thetad_O/T);
aa = [1 LHS_O -LHS_O];
root_finder = roots(aa);
dod_O = root_finder(2,1);
GT_O = LHS_O*rho;
```

```
% Degree of dissociation calculations -- Nitric oxide
LHS_NO = (m_NO/(2*rho))*(Q_tot_atom_NO/Q_tot_mol_NO)*...
    exp(-thetad_NO/T);
aa = [1 LHS_NO -LHS_NO];
root_finder = roots(aa);
dod_NO = root_finder(2,1);
GT_NO = LHS_NO*rho;

% Mixutre of Equilibrium Air (N2, 02, & NO)
% Equilibrium Constants
K_O = 2*k*T*GT_O/m_O;
K_N = 2*k*T*GT_N/m_N;
K_NO = 2*k*T*GT_NO/m_NO;

% Composition of Air (ratio of N_2 to O_2 molecules at STP)
Ratio_air = 4.0;

% Solve system of non-linear equations (5 eqns and 5 unknowns)
clear k_n k_o k_no Pres Air_ratio
syms k_n k_o k_no Pres Air_ratio
eqn1 = 'Pn^2/Pn2-k_n';
eqn2 = 'Po^2/Po2-k_o';
eqn3 = '(Po*Pn)/Pno-k_no';
eqn4 = 'Pres - Pn2-Po2-Pn-Po-Pno';
eqn5 = 'Air_ratio - (2*Pn2+Pn+Pno)/(2*Po2+Po+Pno)';

%Substitute in for pressure and Ratio_air etc.
eqnt1 = subs(eqn1,k_n,K_N);
eqnt2 = subs(eqn2,k_o,K_O);
eqnt3 = subs(eqn3,k_no,K_NO);
eqnt4 = subs(eqn4,Pres,P2);
eqnt5 = subs(eqn5,Air_ratio,Ratio_air);

% Built in function for solving the non-linear system of eqns
A = solve(eqnt1,eqnt2,eqnt3,eqnt4,eqnt5);

% Partial pressure of each species
Pres_Pn2 = double(A.Pn2);
Pres_Pn = double(A.Pn);
Pres_Po2 = double(A.Po2);
Pres_Po = double(A.Po);
Pres_Pno = double(A.Pno);

% Realistic check for partial pressure
% (P can't be less than 0, etc.)
if (real(Pres_Pn2(1,1))>0 && real(Pres_Pn(1,1))>0 && ...
        real(Pres_Po2(1,1))>0 && real(Pres_Po(1,1))>0 && ...
        real(Pres_Pno(1,1)) > 0)
    Pressure_n2 = real(Pres_Pn2(1,1));
    Pressure_n = real(Pres_Pn(1,1));
    Pressure_o2 = real(Pres_Po2(1,1));
    Pressure_o = real(Pres_Po(1,1));
    Pressure_no = real(Pres_Pno(1,1));
end

if (real(Pres_Pn2(2,1))>0 && real(Pres_Pn(2,1))>0 && ...
        real(Pres_Po2(2,1))>0 && real(Pres_Po(2,1))>0 && ...
```

```
        real(Pres_Pno(2,1)) > 0)
    Pressure_n2 = real(Pres_Pn2(2,1));
    Pressure_n = real(Pres_Pn(2,1));
    Pressure_o2 = real(Pres_Po2(2,1));
    Pressure_o = real(Pres_Po(2,1));
    Pressure_no = real(Pres_Pno(2,1));
end

if (real(Pres_Pn2(3,1))>0 && real(Pres_Pn(3,1))>0 && ...
        real(Pres_Po2(3,1))>0 && real(Pres_Po(3,1))>0 && ...
        real(Pres_Pno(3,1)) > 0)
    Pressure_n2 = real(Pres_Pn2(3,1));
    Pressure_n = real(Pres_Pn(3,1));
    Pressure_o2 = real(Pres_Po2(3,1));
    Pressure_o = real(Pres_Po(3,1));
    Pressure_no = real(Pres_Pno(3,1));
end

if (real(Pres_Pn2(4,1))>0 && real(Pres_Pn(4,1))>0 && ...
        real(Pres_Po2(4,1)) > 0 && real(Pres_Po(4,1))>0 && ...
        real(Pres_Pno(4,1)) > 0 )
    Pressure_n2 = real(Pres_Pn2(4,1));
    Pressure_n = real(Pres_Pn(4,1));
    Pressure_o2 = real(Pres_Po2(4,1));
    Pressure_o = real(Pres_Po(4,1));
    Pressure_no = real(Pres_Pno(4,1));
end

% Calculate molar concentrations
xn2 = Pressure_n2/(Pressure_n2+Pressure_n+Pressure_o2+...
    Pressure_o+Pressure_no);
xn = Pressure_n/(Pressure_n2+Pressure_n+Pressure_o2+...
    Pressure_o+Pressure_no);
xo2 = Pressure_o2/(Pressure_n2+Pressure_n+Pressure_o2+...
    Pressure_o+Pressure_no);
xo = Pressure_o/(Pressure_n2+Pressure_n+Pressure_o2+...
    Pressure_o+Pressure_no);
xno = Pressure_no/(Pressure_n2+Pressure_n+Pressure_o2+...
    Pressure_o+Pressure_no);
molar_mass = xn2*28 + xn*14 + xo2*32 + xo*16 + xno*30;

% Calculate mass fractions of each species
cn2 = xn2*28/molar_mass;
cn = xn*14/molar_mass;
co2 = xo2*32/molar_mass;
co = xo*16/molar_mass;
cno = xno*30/molar_mass;

%=========================================================
% Using the above information, now use Fay Riddell relation to
% approximate the stagnation heat transfer to the reentry vehicle.
%=========================================================

Pr = 0.71;                % Prandtl number
Le = 1.4;                 % Lewis number
Hoe = H2+0.5*Rho2*U2^2; % Stagnation (total) enthalpy

% Sutherland's Law - approximate dynamic viscosity
```

```
        mu_e = k_visc*(1.716*10^-5)*(T2/287)^1.5*(287+110.6)/(T2+110.6);

        % Velocity gradient at the wall of the vehicle
        dUedx = (1/Rn)*sqrt(2*(P2-P1)/Rho2);

        % Dissociation enthalpy
        hd = cn*(4.714*10^8)/(14) + co*(2.47*10^8)/(16);

        % Gas constant at the wall (note - for low wall temperature)
        R_mix_w = 287;

        % Density at the wall
        rhow = P2/(R_mix_w*Twall);

        % Enthalpy at the wall
        Hw = Enthalpy_fnct_pres_rho(P2,rhow);

        % Suterhland's Law - dynamic viscosity at the wall
        mu_w = (1.716*10^-5)*(Twall/287)^1.5*(287+110.6)/(Twall+110.6);

        % Equilibrium Heat transfer to the wall
        qdot = 0.76*Pr^-0.6*(Rho2*mu_e)^0.4*(rhow*mu_w)^0.1*sqrt(dUedx)*...
            (Hoe-Hw)*(1+(Le^0.63-1)*hd/Hoe);

        % Convert units to (W/cm^2)
        qwall(q,1) = qdot/10000;
    end

    q = qwall;

    clearvars -except q
```

APPENDIX D

Uncertainty Quantification MATLAB Source Code

```
%==========================================================================
% Author: Ben Bettis
% Date: 2/16/2010
% Purpose: This program propagates mixed aleatory-epistemic
% uncertainties through the Fay-Riddel correlation using
% Second-Order Probability and Non-Intrusive Polynomial Chaos
% response surface fomulation. The final results of the mixed
% uncertainty propagation results in an interval bounds at
% various probability levels for the stagnation point heat
% transfer.
%==========================================================================

format('long'); clear all; close all; clc;
rand('state',0)

% +/- 5% uncertainty in velocity
lower_bound_u1 = 3958.65;
upper_bound_u1 = 4375.35;

% k, epistemic variable, [1,1.15]
lower_bound_k = 1.00;
upper_bound_k = 1.15;

% Initialize the intervals bounds at each probability level
% Note - the large numbers here are meant to be psuedo +/- infinity
ResponseSurf_ProbLevels = [10000000000000000000000000000000000 ...
    -10000000000000000000000000000000000;
10000000000000000000000000000000000  -10000000000000000000000000000000000;
10000000000000000000000000000000000  -10000000000000000000000000000000000;
10000000000000000000000000000000000  -10000000000000000000000000000000000;
10000000000000000000000000000000000  -10000000000000000000000000000000000;
10000000000000000000000000000000000  -10000000000000000000000000000000000];

%==========================================================================
% Point Collocation NIPC

% Order of polynomial chaos
p = 5;

% Number of samples needed (twice the minimum required)
P = 2*((factorial(2+p))/(factorial(2)*factorial(p)));

% Choose samples
M = unifrnd(lower_bound_u1,upper_bound_u1,P,1);  % Velocity
Y = unifrnd(lower_bound_k,upper_bound_k,P,1);    % Mu

% Determine exact solution (RHS of the matrix equation)
for i = 1:P
    RHS(i,1) = Monte_Carlo_Heat_flux_reentry_vehicle(M(i,1),Y(i,1));
end

% Variable transformation
xi_M = (M-lower_bound_u1)/(upper_bound_u1-lower_bound_u1)*2 - 1;
xi_Y = (Y-lower_bound_k)/(upper_bound_k-lower_bound_k)*2 - 1;

psi = zeros(P,P/2);

xi_array(:,1) = xi_M;
```

```
xi_array(:,2) = xi_Y;

for i=1:P
    % psiYi(:,i) = polynomial_test(rand_var_value,[dist_type poly
    % order],# random variables, total_tensor(2) or tailored_tensor(1))
     psi(i,:) = polynomial_combine(xi_array(i,:),[2 p;2 p],2);
end

 % Solve the overdetermined matrix
 coef = psi\RHS;

 % ========================================================================
% !!! Second Order Probability (Mixed uncertainty propagation) !!!
% Fit a surrogate to the data (curve fit). Then use the response
% surface to replace the 'black box' simulation code in 2nd order
% probability. There are two loops in 2nd order probability, an
% inner loop (aleatory UQ) and an outer loop (epistemic UQ). Each
% iteration of the outer loop will produce one CDF curve. Finally,
% the interval bounds for the output variable of interest will be
% found for various probability levels. Note that Second Order
% Probability will use direct Monte Carlo (MC) sampling for the
% inner and outer loops. The function evaluation will come from
% the stochastic response surface formed using NIPC....NOT
% EVALUATING FROM DETERMINISTIC CODE
% ========================================================================

% Now use the surrogate curve fit to do a Monte Carlo simulation
% using Latin Hypercube sampling to get the CDF
n_PostProc_outer = 5000;
n_PostProc_inner = 10000;

% Get the samples from uniform distribution
var_PostProc_Outer = unifrnd(-1,1,n_PostProc_outer,1);

% Initialize a matrix of zeros
ResponseSurf_Array = zeros(n_PostProc_inner,1);
ResponseSurf = zeros(n_PostProc_outer,1);
CDF = zeros(n_PostProc_inner,2);

% Initialize values for the minimum and maximum values in the interval
% bounds at each probability level
MinMax_ResponseSurf = zeros(6,1);

cnt = 0;    % counter for plotting each CDF curve
for i = 1:n_PostProc_outer
    i
    for j = 1:n_PostProc_inner
        var_PostProc_Inner = unifrnd(-1,1,n_PostProc_inner,1);
        % Call MATLAB code to generate basis functions
        BasisFnct = polynomial_combine([var_PostProc_Inner(j,1) ...
            var_PostProc_Outer(i,1)],[2 p;2 p],2);
        sum = 0;
        for k = 1:P/2
            sum = sum + coef(k,1)*BasisFnct(1,k);
        end
        ResponseSurf_Array(j,1) = sum;
    end
    ResponseSurf = sort(ResponseSurf_Array);
```

```
    % CDF curve data
    for m = 1:n_PostProc_inner
        CDF(m,1) = ResponseSurf(m,1);
        CDF(m,2) = m/n_PostProc_inner;
    end

    % Plot every 100th CDF curve
    cnt = cnt + 1;
    if (cnt == 100)
        figure(22)
        set(gca,'FontSize',12,'FontName','Times')
        plot(CDF(:,1),CDF(:,2))
        xlabel('Heat Transfer (W/cm^2)', 'FontSize', 16)
        ylabel('CDF', 'FontSize', 16)
        hold on
        cnt = 0;
        dlmwrite('CDF_multipleCurves_uniform.dat',CDF,'-append')
    end

    % Find the min and max values in interval bounds for each probability
    % level
    multiplier = 0.0;
    for level_cnt = 1:6
        if (level_cnt == 1)
            MinMax_ResponseSurf(level_cnt,1) = ResponseSurf(1,1);
            multiplier = multiplier + 0.2;
        else
            MinMax_ResponseSurf(level_cnt,1) = ...
                ResponseSurf(round(multiplier*n_PostProc_inner),1);
            multiplier = multiplier + 0.2;
        end
    end

    % Replace the "overall" minimum and max values in the
    % interval bounds at each probability level
        for level_cnt = 1:6
            if (MinMax_ResponseSurf(level_cnt,1) > ...
                    ResponseSurf_ProbLevels(level_cnt,2))
                CDF_max = CDF;
                ResponseSurf_ProbLevels(level_cnt,2) = ...
                    MinMax_ResponseSurf(level_cnt,1);
            end
            if (MinMax_ResponseSurf(level_cnt,1) < ...
                    ResponseSurf_ProbLevels(level_cnt,1))
                CDF_min = CDF;
                ResponseSurf_ProbLevels(level_cnt,1) = ...
                    MinMax_ResponseSurf(level_cnt,1);
            end
        end

end

% Plot the minimum and maximum CDF curves on the same plot
figure(33)
set(gca,'FontSize',12,'FontName','Times')
plot(CDF_min(:,1),CDF_min(:,2),'r',CDF_max(:,1),CDF_max(:,2),'b')
xlabel('Heat Transfer (W/cm^2)', 'FontSize', 16)
```

```
ylabel('CDF', 'FontSize', 16)

% Write the CDF curve data to an external file
dlmwrite('Fay_Riddell_Epistemic_Results_uniform_Max_CDFCurves.dat'...
    ,CDF_max)
dlmwrite('Fay_Riddell_Epistemic_Results_uniform_Min_CDFCurves.dat',...
    CDF_min)
```

BIBLIOGRAPHY

[1] F. S. Milos and D.J. Rasky. Review of numerical procedures for computational surface thermochemistry. *Journal of Thermophysics and Heat Transfer*, 8(1):24–34, 1994.

[2] M. MacLean, E. Mundy, T. Wadhams, M. Holden, and R. Parker. Analysis and ground test of aerothermal effects on spherical capsule geometries, AIAA-paper 2008-4273. In 38^{th} *AIAA Fluid Dynamics Conference and Exhibit*, Seattle, WA, June 23-26, 2009.

[3] D. Bose and M. Wright. Uncertainty analysis of laminar aeroheating predictions for mars entries, AIAA-paper 2005-4682. In 38^{th} *AIAAThermophysics Conference*, Toronto, Ontario Canada, 2005.

[4] D. Bose, M. Wright, and T. Gökçen. Uncertainty and sensitivity analysis of thermochemical modeling for titan atmospheric entry, AIAA-paper 2004-2455. In 37^{th} *AIAAThermophysics Conference*, Portland, OR, 2004.

[5] A. Weaver, A Alexeenko, R. Greendyke, and J. Camberos. Flowfield uncertainty analysis for hypersonic cfd simulations, AIAA-paper 2010-1180. In 48^{th} *AIAAAerospace Sciences Meeting*, Orlando, FL, Jan. 4-7, 2010.

[6] S. Ghaffari, T. Magin, and G. Iaccarino. Uncertainty quantification of radiative heat flux modeling for titan atmospheric entry, AIAA-paper 2010-239. In 48^{th} *AIAAAerospace Sciences Meeting*, Orlando, FL, Jan. 4-7, 2010.

[7] W. L. Oberkampf, J. C. Helton, and K. Sentz. Mathematical representation of uncertainty, AIAA-paper 2001-1645. In 3^{rd} *Non-Deterministic Approaches Forum*, Seattle, WA, April, 2001.

[8] M. Eldred and L. Swiler. Efficient algorithms for mixed aleatory-epistemic uncertainty quantification with application to radiation-hardened electronics. *Sandia National Laboratories Report*, SAND2009-5805, September, 2009.

[9] L. Swiler, T. Paez, R. Mayes, and M. Eldred. Epistemic uncertainty in the calculation of margins, AIAA-paper 2009-2249. In 50^{th} *AIAA/ASME/ASCE/AHS/ASC Structures, Structural Dynamics, and Materials Conference*, Palm Springs, CA, May4-7, 2009.

[10] S. Hosder and R. Walters. Non-intrusive polynomial chaos methods for stochastic cfd theory and applications. In *Symposium on Computational Uncertainty in Military Vehicle Design NATO Applied Vehicle Technology Panel, Paper No. 47*, Athens, Greece, December, 2007.

[11] S. Hosder and R. W. Walters. Non-intrusive polynomial chaos methods for uncertainty quantification in fluid dynamics, AIAA-paper 2010-0129. In 48^{th} *AIAA Aerospace Sciences Meeting*, Orlando, FL, January 4-7, 2010.

[12] L. P. Swiler and A. A. Giunta. Aleatory and epistemic uncertainty quantification for engineering applications. *Sandia National Laboratories Report*, SAND2007-2670C, July, 2007.

[13] J. Guo and X. Du. Reliability analysis for multidisciplinary systems with random and interval variables, AIAA-paper 2008-1984. In 49^{th} *AIAA/ASME/ASCE/AHS/ASC Structures, Structural Dynamics, and Materials Conference*, Schaumburg, IL, April 7-10, 2008.

[14] J. Guo and X. Du. Reliability sensitivity analysis with random and interval variables. *International Journal for Numerical Methods in Engineering*, 2008.

[15] X. Du, A. Sudjianto, and B. Huang. Reliability-based design under the mixture of random and interval variables. *ASME Journal of Mechanical Design*, 2005.

[16] D. R. Karanki, H. S. Kushwaha, A. K. Verma, and S. Ajit. Uncertainty analysis based on probability bounds (p-box) approach in probabilistic safety assessment. *Risk Analysis*, 2009.

[17] J. Jakeman, M. Eldred, and D. Xiu. Numerical approach for quantification of epistemic uncertainty. *Journal of Computational Physics*, 2010.

[18] M. S. Eldred. Recent advances in non-intrusive polynomial chaos and stochastic collocation methods for uncertainty analysis and design, AIAA-paper 2009-2274. In 50^{th} *AIAA/ASME/ASCE/AHS/ASC Structures, Structural Dynamics, and Materials Conference*, Palm Springs, CA, May 4-7, 2009.

[19] B. Bettis and S. Hosder. Quantification of uncertainty in aerodynamic heating of a reentry vehicle due to uncertain wall and freestream conditions, AIAA-paper 2010-4642. In 10^{th} *AIAA/ASME Joint Thermophysics and Heat Transfer Conference*, Chicago, IL, June, 2010.

[20] W. L. Oberkampf and J. C. Helton. Investigation of evidence theory for engineering applications, AIAA-paper 2002-1569. In 4^{th} *Non-Deterministic Approaches Forum*, Denver, CO, Ajpril, 2002.

[21] N. Wiener. The homogeneous chaos. *American Journal of Mathematics*, 60(4):897–936, 1994.

[22] D. Xiu and G. E. Karniadakis. Modeling uncertainty in flow simulations via generalized polynomial chaos. *Journal of Computational Physics*, 187(1):137–167, May, 2003.

[23] L. Huyse, A. R. Bonivtch, J. B. Pleming, D. S. Riha, C. Waldhart, and B. H. Thacker. Verification of stochastic solutions using polynomial chaos expansions, AIAA-paper 2006-1994. In 47^{th} *AIAA/ASME/ASCE/AHS/ASC Structures, Structural Dynamics, and Materials Conference*, Newport, RI, May, 2006.

[24] M. S. Eldred, C. G. Webster, and P. G. Constantine. Evaluation of non-intrusive approaches for wiener-askey generalized polynomial chaos, AIAA-paper 2008-1892. In 10^{th} *AIAA Non-Deterministic Approaches Forum*, Schaumburg, IL, April, 2008.

[25] R. W. Walters and L. Huyse. Uncertainty analysis for fluid mechanics with applications. Technical report, ICASE 2002-1, NASA/CR-2002-211449, NASA Langley Research Center, Hampton, VA, 2002.

[26] H. N. Najm. Uncertainty quantification and polynomial chaos techniques in computational fluid dynamics. *Annual Review of Fluid Mechanics*, 41:35–52, 2009.

[27] S. Hosder, R. W. Walters, and M. Balch. Efficient sampling for non-intrusive polynomial chaos applications with multiple input uncertain variables, AIAA-paper 2007-1939. In 9^{th} *AIAA Non-Dterministic Approaches Conference*, Honolulu, HI, April, 2007.

[28] J. A. Fay and F. R. Riddell. Theory of stagnation point heat transfer in dissociated air. *Journal of Aeronautical Sciences*, 25(25):73–85, February, 1958.

[29] John D. Anderson. *Hypersonics and High-Temperature Gas Dynamics, Second Edition*. AIAA, Reston, VA, 2006.

[30] S. Srinivasan, J. Tannehill, and K. Weilmuenster. Simplified curve fits for the thermodynamic properties of equilibrium air. *NASA Reference Publication 1181*, 1987.

[31] W. G. Vincenti and C. H. Kruger. *Introduction to Physical Gas Dynamics*. Krieger Publishing Company, Malabar, FL, 1965.

[32] J.C. Helton, J.D. Johnson, C.J. Sallaberry, and C.B. Storlie. Survey of smapling-based methods for uncertainty and sensitivity analysis. *Reliability Engineering and System Safety*, 2006.

[33] *GASP User Manual*. AeroSoft, Inc., Blacksburg, Virginia, 1997.

[34] D. A. Steward, Y. K. Chen, and W. D. Henline. Effect of non-equilibrium flow chemistry and surface catalysis on surface heating to afe, AIAA-paper 91-1373. In 26^{th} *AIAAThermophysics Conference*, Honolulu, Hawaii, June 24-26, 1991.

[35] P. Kolodziej and D. A. Steward. Nitrogen recomibnation on high-temperature reusable surface insulation and the analysis of its effect on surface catalyis, AIAA-paper 87-1637. June 1987.

[36] D. A. Steward and P. Kolodziej. Wall catalysis experiment on afe, AIAA-paper 88-2674. June 1988.

[37] C. Park. Assessment of two-temperature kinetic model for ionizing air. *Journal of Thermophysics and Heat Transfer*, 3(3):233–244, 1989.

[38] R. C. Millikan and D. R. White. Systematics of vibrational relaxation. *Journal of Chemical Physics*, 39(12), 1963.

[39] R. N. Gupta, J. M. Yos, R. A. Thompson, and K. P. Lee. A review of reaction rates and thermodynamic and transport properties for an 11-species air model for chemical and thermal nonequilibrium calculations to 30,000°k. *NASA RP-1232*, 1990.

[40] I.M. Sobol'. Global sensitivity indices for nonlinear mathematical models and their monte carlo estimates. *Mathematics and Computers in Simulation*, 55:271–280, 2001.

[41] T. Crestaux, O.L. Maître, and J-M Martinez. Polynomial chaos expansion for sensitivity analysis. *Reliabiilty Engineering and System Safety*, 2009.

VITA

Benjamin Robert Bettis was born in St. Louis, Missouri. He lived in Cedar Hill, MO for the first ten years of his life and then moved to Hillsboro, MO where he continued to live through high school. After graduating from Hillsboro High School in 2005, he started his undergraduate career at the University of Missouri-Rolla studying Aerospace Engineering. During this time, he was an active member of Sigma Gamma Tau and served as president for the American Institute of Aeronautics and Astronautics chapter. He also participated in the Opportunities for Undergraduate Research Experience program and the Missouri Space Grant Consortium working for Dr. Fathi Finaish. In the winter of 2007, he began conducting research under Dr. Serhat Hosder and has continued working with him throughout his graduate career. He completed his Bachelor of Science degree in Aerospace Engineering in the spring of 2009 and graduated with Summa Cum Laude honors. He then received his Master of Science Degree in Aerospace Engineering at the Missouri University of Science and Technology in December 2010.